

Deep importance sampling using tensor-trains with application to *a priori* and *a posteriori* rare event estimation

BY TIANGANG CUI

School of Mathematics, Monash University, Victoria 3800, Australia
tiangang.cui@monash.edu

SERGEY DOLGOV

Department of Mathematical Sciences, University of Bath, Bath, BA2 7AY, UK
s.dolgov@bath.ac.uk

ROBERT SCHEICHL

*Institute for Applied Mathematics and Interdisciplinary Center for Scientific Computing,
Heidelberg University, Im Neuenheimer Feld 205, 69120 Heidelberg, Germany*
r.scheichl@uni-heidelberg.de

SUMMARY

We propose a deep importance sampling method that is suitable for estimating rare event probabilities in high-dimensional problems. We approximate the optimal importance distribution in a general importance sampling problem as the pushforward of a reference distribution under a composition of order-preserving transformations, in which each transformation is formed by a squared tensor-train decomposition. The squared tensor-train decomposition provides a scalable ansatz for building order-preserving high-dimensional transformations via density approximations. The use of composition of maps moving along a sequence of bridging densities alleviates the difficulty of directly approximating concentrated density functions. To compute expectations over unnormalized probability distributions, we design a ratio estimator that estimates the normalizing constant using a separate importance distribution, again constructed via a composition of transformations in tensor-train format. This offers better theoretical variance reduction compared with self-normalized importance sampling, and thus opens the door to efficient computation of rare event probabilities in Bayesian inference problems. Numerical experiments on problems constrained by differential equations show little to no increase in the computational complexity with the event probability going to zero, and allow to compute hitherto unattainable estimates of rare event probabilities for complex, high-dimensional posterior densities.

Some key words: Rare events, Bayesian inference, importance sampling, tensor-train, transport maps

1. INTRODUCTION

In the analysis of many scientific and engineering systems, practitioners often assess the performance and the inherent uncertainty using expectations of functions of random variables or random processes. As a starting point, the potential sources of input uncertainty in the system are parametrized by some random variable and equipped with a prior distribution. Then, given some model that maps the uncertain parameters to observables, the *a priori* uncertainty can be reduced to the *a posteriori* uncertainty by conditioning on observed data to obtain the posterior distribution under the Bayesian framework. Depending on the availability of data, accurate estimates of *a priori* and *a posteriori* expectations of some output functionals are both of interest.

Analytical or asymptotic characterizations of the abovementioned expectations are often unavailable, because of non-analytically tractable posterior distributions, nonlinear functions of interests, or a combination of both. Thus, numerical techniques such as Monte Carlo methods must be employed. Importance sampling provides a general tool to efficiently compute expectations of this sort by allocating computational resources to the “important” regions of the expectation problem. In the literature, adaptive importance sampling strategies have been developed to iteratively identify the important region and also to adaptively estimate importance distributions in some parametric family, e.g., mixture distributions (Oh & Berger, 1993; Del Moral et al., 2006; Douc et al., 2007; Cappé et al., 2008; Cornuet et al., 2012; Li et al., 2013). In general, the construction of importance distributions in high dimensions is challenging, especially when the important region localizes to the tail of the input distribution, as we may not be able to accurately approximate the optimal importance distribution using parametric families. As a result, the mean square error of an importance sampling estimator may deteriorate quickly, sometimes exponentially, as the parameter dimension increases. This becomes even more critical for rare event problems, where the rather small event probability, often on a scale of 10^{-6} or less, requires an accurate approximation to the optimal importance distribution, so that the relative mean square error can be controlled for a fixed computational budget.

We present a deep importance sampling scheme that is suitable for high-dimensional rare event problems. It employs the deep inverse Rosenblatt transport developed in Dolgov et al. (2020) and Cui & Dolgov (2021) to adaptively approximate the optimal importance density using a composition of order-preserving maps. When the optimal importance density is multi-modal and concentrated in the tails of the input distribution, the composite structure is able to adapt to those complicated features. Each of the maps in the composition is constructed using functional tensor-train (TT) decomposition and the cross algorithm (Oseledets & Tyrtshnikov, 2010; Oseledets, 2011; Hackbusch, 2012; Bigoni et al., 2016; Gorodetsky et al., 2019). It provides a non-parametric ansatz for approximating the optimal importance density. Thus, it can be significantly more accurate than alternative importance sampling densities based on mixture distributions. In addition, for problems with sufficient regularity, the accuracy of tensor-train approximations can be independent of the parameter dimension; see Griebel & Harbrecht (2021) for details. The computational complexity of building tensor-train decompositions and the resulting transport maps scales linearly in the dimension. The proposed importance sampling scheme is further extended to handle input probability distributions with unknown normalizing constants, so it can be applied to estimate *a posteriori* expectations. Crucially, it is possible to construct a significantly more effective estimator than the familiar self-normalized importance sampling scheme, by constructing an additional importance density, again based on the deep inverse Rosenblatt transport framework, but now targeting the optimized importance density for the normalizing constant.

To demonstrate the power of the proposed deep importance sampling, we present non-trivial applications in risk assessment of spatial, susceptible-infectious-removed models and contaminant transport in groundwater systems in the challenging regime of rare events. Our numerical results suggest that the proposed method can accurately estimate both *a priori* and *a posteriori* expectations using several orders of magnitude smaller sample sizes compared to importance densities based on mixtures distributions. More importantly, the use of composition of maps and tensor-train decomposition allows us to estimate rare event probabilities in high dimensions so far intractable by standard importance sampling methods.

2. BACKGROUND

We consider a random variable X taking values in $\mathcal{X} \subseteq \mathbb{R}^d$ and assign a prior probability density π_0 to it. Given an integrable function $f : \mathcal{X} \rightarrow \mathbb{R}$, our goal is to estimate the expectation $F = E_{\pi_0}\{f(X)\}$. Importance sampling methods approach this goal by choosing a suitable importance density p , satisfying the sufficient condition $\text{supp}(f\pi_0) \subseteq \text{supp}(p)$, and then estimating $E_p\{f(X)\pi_0(X)/p(X)\}$ instead. Drawing N independent and identically distributed samples from p , one can construct the *unbiased im-*

importance sampling estimator of F :

$$\hat{F}_{p,N} = \frac{1}{N} \sum_{i=1}^N \frac{f(X^i) \pi_0(X^i)}{p(X^i)}, \quad X^i \sim p. \quad (1)$$

The performance of the estimator $\hat{F}_{p,N}$ is measured using the relative mean square error,

$$\text{rmse}(\hat{F}_{p,N}, F) = \frac{E\{(\hat{F}_{p,N} - F)^2\}}{F^2} = \frac{\text{var}_p(\hat{F}_{p,N})}{F^2} + \frac{|E(\hat{F}_{p,N}) - F|^2}{F^2}, \quad (2)$$

where $\text{var}_p(g) = E_p\{g(X)^2\} - E_p\{g(X)\}^2$ gives the variance of a function $g : \mathcal{X} \rightarrow \mathbb{R}$ with respect to the density p . The relative mean square error (2) is minimized for any given sample size N by choosing the *optimal* importance density $p^* \propto |f|\pi_0$ that minimizes $\text{var}_p(f\pi_0/p)$ over all densities p with $\text{supp}(f\pi_0) \subseteq \text{supp}(p)$. If the function of interest $f(x)$ is non-negative on \mathcal{X} , then we have $\text{var}_{p^*}(f\pi_0/p^*) = 0$, which leads to a *zero-variance* estimator.

Given observed data $y \in \mathcal{Y} \subseteq \mathbb{R}^m$, under the Bayesian paradigm, the likelihood function $x \mapsto \mathcal{L}^y(x)$ updates the prior distribution π_0 on X to the posterior distribution with density

$$\pi^y(x) = \frac{1}{Z} \mathcal{L}^y(x) \pi_0(x), \quad Z = E_{\pi_0}\{\mathcal{L}^y(X)\}, \quad (3)$$

where Z is the normalizing constant. Conditioned on observed data, the central goal of the paper is to estimate the *a posteriori* expectation

$$R = E_{\pi^y}\{f(X)\} = \frac{1}{Z} \int_{\mathcal{X}} f(x) \mathcal{L}^y(x) \pi_0(x) dx. \quad (4)$$

The *a posteriori* setting adds additional challenges. In particular, simulating independent and identically distributed random variables from the posterior is often impossible and the normalizing constant Z is typically unknown. Since the posterior expectation can be written as the ratio

$$R = \frac{E_{\pi_0}\{f(X)\mathcal{L}^y(X)\}}{E_{\pi_0}\{\mathcal{L}^y(X)\}}, \quad (5)$$

an alternative importance sampling estimator can be constructed by carefully selecting two importance densities p and q such that $\text{supp}(f\pi) \subseteq \text{supp}(p)$ and $\text{supp}(\pi) \subseteq \text{supp}(q)$ to estimate the numerator and the denominator of (5), which now can be equivalently written as

$$Q = E_p\left\{\frac{f(X)\mathcal{L}^y(X)\pi_0(X)}{p(X)}\right\}, \quad Z = E_q\left\{\frac{\mathcal{L}^y(X)\pi_0(X)}{q(X)}\right\}, \quad (6)$$

respectively. Drawing independent and identically distributed samples $X_p^i \sim p$ and $X_q^i \sim q$, we can construct unbiased importance sampling estimators

$$\hat{Q}_{p,N} = \frac{1}{N} \sum_{i=1}^N \frac{f(X_p^i) \mathcal{L}^y(X_p^i) \pi_0(X_p^i)}{p(X_p^i)}, \quad \hat{Z}_{q,N} = \frac{1}{N} \sum_{i=1}^N \frac{\mathcal{L}^y(X_q^i) \pi_0(X_q^i)}{q(X_q^i)}, \quad (7)$$

to estimate Q and Z , respectively. This leads to the *ratio estimator*

$$\hat{R}_{p,q,N} := \frac{\hat{Q}_{p,N}}{\hat{Z}_{q,N}}, \quad (8)$$

for the *a posteriori* expectation. Note that although both $\hat{Q}_{p,N}$ and $\hat{Z}_{q,N}$ are unbiased, the ratio estimator $\hat{R}_{p,q,N}$ is in general biased. We will discuss the impact of this bias in later sections.

A computationally convenient choice is the so-called *self-normalized importance sampling estimator* with $p = q$. However, the respective optimal importance densities $p^* \propto |f|\mathcal{L}^y\pi_0$ and $q^* = \pi^y$ for Q and Z may differ significantly for challenging problems, e.g., when the function of interest f only takes

significant values in the tail of the posterior density π^y . We propose to construct separate, near-optimal importance densities p and q to reduce the overall relative mean square error of the ratio estimator (8).

A particular application is the estimation of failure probabilities of physical or engineering systems to assess their reliability or to inform policy makers. Given a response function $h : \mathcal{X} \mapsto \mathbb{R}$, system failure is characterized by determining whether the output of h falls inside of a set $\mathcal{A} \subset \mathbb{R}$ or not. Thus, the function of interest representing a system failure becomes

$$f(x) = \mathbf{1}_{\mathcal{A}}\{h(x)\} \quad (9)$$

where $\mathbf{1}_{\mathcal{A}}(\cdot)$ denotes the indicator function of the set \mathcal{A} . Depending on the availability of data, both the *a priori* and the *a posteriori* failure probabilities,

$$\text{pr}_{\pi_0}\{h(X) \in \mathcal{A}\} = E_{\pi_0}\{f(X)\}, \quad \text{pr}_{\pi^y}\{h(X) \in \mathcal{A}\} = E_{\pi^y}\{f(X)\}, \quad (10)$$

provide risk assessment criteria associated with the response function h . Estimating those probabilities is particularly challenging when the failure set $\mathcal{X}_F := \{x \in \mathcal{X} : f(x) = 1\}$ has a very small probability mass, also referred to as a *rare event*.

Most of the existing literature for complex high-dimensional applications focuses on estimating *a priori* failure probabilities (e.g., [Elfverson et al., 2016](#); [Peherstorfer et al., 2016, 2018](#); [Uribe et al., 2021](#); [Wagner et al., 2020](#); [Dodwell et al., 2021](#)), while our approach applies equally to *a posteriori* failure probabilities and clearly outperforms the classical cross entropy method ([Botev & Kroese, 2008](#)); see Sections 4–6 for the setup and numerical examples.

3. DEEP IMPORTANCE SAMPLING USING TENSOR-TRAINS

3.1. Problem setup

To encompass both *a priori* and *a posteriori* expectations the optimal importance density is presented in the general form of

$$p^*(x) = \frac{1}{\zeta^*} \rho^*(x), \quad \zeta^* = \int_{\mathcal{X}} \rho^*(x) dx, \quad (11)$$

where $\rho^*(x)$ is the unnormalized optimal importance density and ζ^* is the normalizing constant. This includes *a priori* expectations, where $\rho^* = |f|\pi_0$, as well as the numerator and the denominator of the ratio estimator (8) for *a posteriori* expectations, where $\rho^* = |f|\mathcal{L}^y\pi_0$ and $\rho^* = \mathcal{L}^y\pi_0$, respectively. For the remainder we assume that ζ^* is unknown and that we can only evaluate the unnormalized density ρ^* .

Our ultimate goal is to build a normalized approximation to the optimal p^* as the pushforward of an analytically tractable and product-form reference density $\lambda(x) = \prod_{k=1}^d \lambda_k(x_k)$ under an order-preserving map $\mathcal{T} : \mathbb{R}^d \rightarrow \mathbb{R}^d$. Then, the resulting transformation can be used to generate independent and identically distributed random variables for importance sampling. We make the following assumptions about the importance sampling problem:

Assumption 1. The function of interest f is non-negative.

Assumption 2. The ratio ρ^*/π_0 has finite mean and finite second moment with respect to π_0 .

Assumption 3. There exists a reference density λ satisfying $\sup_{x \in \mathcal{X}} \pi_0(x)/\lambda(x) < \infty$.

Assumption 1 holds for the failure probability problem, which is our main application. By focusing on non-negative f , the optimal importance density leads to a zero-variance estimator. Thus, our goal is to design importance densities that closely approximate the optimal density to provide *near zero-variance* estimators. However, our discussion can easily be extended to general functions. One can decompose any function f as the difference of two non-negative functions $f(x) = f_+(x) - f_-(x)$, where $f_+(x) = f(x)\mathbf{1}_{\{f(x) > 0\}}(x)$ and $f_-(x) = f(x)\mathbf{1}_{\{f(x) \leq 0\}}(x)$. The original expectation $E_{\pi_0}\{f(X)\}$ can then be computed from $E_{\pi_0}\{f_+(X)\} - E_{\pi_0}\{f_-(X)\}$, if both f_+ and f_- are integrable.

Assumption 2 guarantees that the nominal estimator, which uses the prior density π_0 as the importance density, satisfies the assumptions of the central limit theorem. We adopt this assumption to analyse the relative mean square error of our proposed estimators. Assumption 3 is introduced to ensure $\text{supp}(\rho^*) \subseteq \text{supp}(\lambda)$ for all the cases of interest specified at the start of Section 3.1. Then λ can be used as reference density to avoid any potential singularities in approximating the optimal importance density. In most cases, λ will be the prior density.

3.2. From tensor-trains to squared inverse Rosenblatt transport

The central tool in our new approach is an approximation of the square root of the unnormalized optimal importance density ρ^* in a functional tensor-train (TT) decomposition

$$\sqrt{\rho^*}(x) \approx \tilde{g}(x) = \mathbf{G}_1(x_1) \cdots \mathbf{G}_k(x_k) \cdots \mathbf{G}_d(x_d), \quad (12)$$

where each of the $\mathbf{G}_k(x_k)$ is a matrix-valued function of size $r_{k-1} \times r_k$, with $r_0 = r_d = 1$. Using a representation of $\sqrt{\rho^*}$ in tensor product form with n_k basis functions in the k th coordinate, such a tensor-train decomposition can be computed very efficiently without incurring the curse of dimensionality for a wide range of densities via alternating linear schemes together with cross approximation (Oseledets & Tyrtyshnikov, 2010; Bigoni et al., 2016; Gorodetsky et al., 2019). In this work, we employ the functional extension of the alternating minimal energy method with residual-based rank adaptation of Dolgov & Savostyanov (2014). It requires only $\mathcal{O}(dnr^2)$ evaluations of the density ρ^* and $\mathcal{O}(dnr^3)$ floating point operations, where $n = \max_k n_k$ and $r = \max_k r_k$. For more details see Dolgov et al. (2020) and Cui & Dolgov (2021). In general, the maximal rank r depends on the dimension d and can be large when the density ρ^* concentrates in some part of its domain, but some theoretical results exist that provide rank bounds. While Rohrbach et al. (2022) establish specific bounds for certain multivariate Gaussian densities that depend poly-logarithmically on d , Griebel & Harbrecht (2021) prove dimension-independent bounds for general functions in weighted spaces with dominating mixed smoothness.

Given such a tensor-train decomposition of $\sqrt{\rho^*}$, an approximation to the normalized optimal importance density, can be computed from

$$p(x) = \frac{1}{\zeta} \rho(x), \quad \rho(x) = \tilde{g}(x)^2 + \tau \lambda(x), \quad \zeta = \int_{\mathcal{X}} \{\tilde{g}(x)^2 + \tau \lambda(x)\} dx, \quad (13)$$

for some $\tau > 0$. The additional term $\tau \lambda(x)$ guarantees that $\text{supp}(\rho^*) \subseteq \text{supp}(p)$, and thus the importance sampling estimator defined by the approximate density p is unbiased. The following lemma, whose original proof is given in Cui & Dolgov (2021), shows how to choose τ as a function of the error in \tilde{g} in the L^2 -norm, to be able to control the overall error of the approximate density p in Hellinger distance.

LEMMA 1. *Suppose $\|\sqrt{\rho^*} - \tilde{g}\|_2 \leq \epsilon$ and $\tau \leq \epsilon^2$. Then, the exact normalizing constant ζ^* in (11) and its approximation ζ in (13) satisfy $|\zeta^* - \zeta| \leq \sqrt{2}\epsilon$ and the Hellinger distance between p^* and its normalized approximation p defined in (13) can be bounded by $D_H(p^*, p) \leq 2\epsilon/\sqrt{\zeta^*}$.*

DEFINITION 1. *For any vector $x \in \mathbb{R}^d$ and any index $k \in \{1, \dots, d\}$, the first $k - 1$ coordinates and the last $d - k$ coordinates of x are expressed as $x_{<k} = [x_1, \dots, x_{k-1}]^\top$ and $x_{>k} = [x_{k+1}, \dots, x_d]^\top$, respectively. Similarly, we write $x_{\leq k} = (x_{<k}, x_k)$, $x_{\geq k} = (x_k, x_{>k})$, $x_{\leq 1} = x_1$, $x_{\geq d} = x_d$, and $x_{\leq d} = x$.*

Following Dolgov et al. (2020) and Cui & Dolgov (2021), to build an efficient sampling method based on this density approximation we now build an order-preserving map $\mathcal{Q} : \mathbb{R}^d \rightarrow \mathcal{X}$, the generalized inverse Rosenblatt transport, such that the pushforward of the reference density λ under the map \mathcal{Q} is the normalized approximate density p , i.e., $\mathcal{Q}_\# \lambda = p$. Exploiting the separable structure of the tensor-train approximation \tilde{g} , the unnormalized marginal densities

$$\rho_{\leq k}(x_{\leq k}) = \int_{\mathcal{X}_{>k}} \rho(x_{\leq k}, x_{>k}) dx_{>k} = \int_{\mathcal{X}_{>k}} \tilde{g}(x_{\leq k}, x_{>k})^2 dx_{>k} + \tau \lambda_{\leq k}(x_{\leq k}), \quad (14)$$

with $\lambda_{\leq k}(x_{\leq k}) = \prod_{j=1}^k \lambda_j(x_j)$ for $1 \leq k < d$, can be computed analytically via a sequence of one-dimensional integrations. Finally, by integrating the one-dimensional unnormalized marginal density

$\rho_{\leq 1}(x_1)$ one more time, we obtain the normalizing constant ζ . We provide the details of this marginalization procedure in [Appendix B](#).

The normalized densities for the marginal random variables $X_{\leq k}$, $1 \leq k < d$, are thus given by $p_{\leq k}(x_{\leq k}) = \zeta^{-1} \rho_{\leq k}(x_{\leq k})$. Now, the joint random variable X can be equivalently expressed as a one-dimensional marginal and a sequence of $d - 1$ one-dimensional conditional random variables, $X_1, X_2 | X_{< 2}, \dots, X_d | X_{< d}$, with distribution functions

$$\mathcal{F}_{\leq 1}(x_1) = \int_{-\infty}^{x_1} p_{\leq 1}(x'_1) dx'_1, \quad \mathcal{F}_{k|<k}(x_k | x_{<k}) = \int_{-\infty}^{x_k} \frac{p_{\leq k}(x_{<k}, x'_k)}{p_{<k}(x_{<k})} dx'_k, \quad (15)$$

respectively. This defines the *Rosenblatt transport* according to [Rosenblatt \(1952\)](#),

$$\xi = \begin{bmatrix} \xi_1 \\ \vdots \\ \xi_d \end{bmatrix} = \begin{bmatrix} \mathcal{F}_{\leq 1}(x_1) \\ \vdots \\ \mathcal{F}_{d|<d}(x_d | x_{<d}) \end{bmatrix} = \mathcal{F}(x). \quad (16)$$

Given $X \sim p$, the random variable $\Xi = \mathcal{F}(X)$ is distributed uniformly in the unit hypercube $[0, 1]^d$. Since the k -th component of \mathcal{F} is a scalar valued function $\mathcal{F}_{k|<k} : \mathbb{R}^k \mapsto \mathbb{R}$, depending on the first k variables only, the map \mathcal{F} has a *lower-triangular* form.

The reason for decomposing the square root $\sqrt{\rho^*}$ of the unnormalized importance density instead of ρ^* becomes apparent here. Directly decomposing the density ρ^* using tensor-trains, the non-negativity of the approximated density function can not be guaranteed due to rank truncation. Approximating $\sqrt{\rho^*}$ preserves non-negativity without any loss of smoothness in the resulting approximate density ρ and in all marginal densities $\rho_{\leq k}$, $1 \leq k < d$. Crucially, it also guarantees that all one-dimensional distribution functions in (15) are monotonically increasing and that the map \mathcal{F} , as well as its inverse are order-preserving and almost surely differentiable.

Let μ denote the uniform density on $[0, 1]^d$. Then the pullback of μ under the map \mathcal{F} satisfies

$$\mathcal{F}^\# \mu(x) = \mu(\mathcal{F}(x)) |\nabla_x \mathcal{F}(x)| = |\nabla_x \mathcal{F}(x)| = p(x).$$

Since the product-form reference density $\lambda(u)$ is naturally equipped with the diagonal map

$$\xi = \mathcal{R}(u) = [\mathcal{R}_1(u_1), \dots, \mathcal{R}_k(u_k), \dots, \mathcal{R}_d(u_d)]^\top, \quad \mathcal{R}_k(u_k) = \int_{-\infty}^{u_k} \lambda_k(u'_k) du'_k,$$

such that $\mathcal{R}_\# \lambda = \mu$, the composite map $\mathcal{Q} = \mathcal{F}^{-1} \circ \mathcal{R}$ also has the lower-triangular structure and satisfies $\mathcal{Q}_\# \lambda = p$. Thus, one can first generate random variables $U \sim \lambda$, distributed according to the reference density λ , and then apply the *general inverse Rosenblatt transport* $X = \mathcal{Q}(U)$ to obtain a random variable $X \sim p$. The map $\mathcal{Q} : \mathbb{R}^d \rightarrow \mathcal{X}$ is again *lower-triangular* and can be evaluated successively as

$$x = \left[\mathcal{F}_{\leq 1}^{-1}\{\mathcal{R}_1(u_1)\}, \dots, \mathcal{F}_{d|<d}^{-1}\{\mathcal{R}_d(u_d) | x_{<d}\} \right]^\top. \quad (17)$$

Thus defined *squared inverse Rosenblatt transport* can be also used as an efficient *conditional distribution method* in the classical sense, see, e.g., [Johnson \(1987\)](#).

3.3. From inverse Rosenblatt transport to deep importance sampling

For problems such as rare event estimation, the optimal importance density can concentrate to a small region of the parameter space, or even to a sub-manifold, due to complex nonlinear interactions. In this situation, constructing in one step a tensor-train approximation of $\sqrt{\rho^*}$ may result in rather high tensor ranks. It can also be challenging to find an appropriate basis to efficiently discretize $\sqrt{\rho^*}$ in each coordinate direction, by adapting to high-probability regions of the optimal importance density. As a consequence, both r and n can become very large.

We propose to overcome this difficulty by building a composition of maps

$$\mathcal{T}^{(L)} = \mathcal{Q}^{(1)} \circ \mathcal{Q}^{(2)} \circ \dots \circ \mathcal{Q}^{(L)},$$

that can adapt to a concentrated optimal importance density layer-by-layer. The adaptive construction is guided by a sequence of unnormalized bridging densities

$$\phi^{(1)}, \phi^{(2)}, \dots, \phi^{(L)} \equiv \rho^*$$

with increasing complexity. To specify the adaptation, we denote the ℓ th normalized bridging density as

$$\varphi^{(\ell)}(x) = \frac{1}{\omega^{(\ell)}} \phi^{(\ell)}(x), \quad \omega^{(\ell)} = \int_{\mathcal{X}} \phi^{(\ell)}(x) dx.$$

At any layer ℓ , the pushforward of the reference density λ under the partial composition $\mathcal{T}^{(\ell)}$ is constructed such that it approximates the ℓ th normalized bridging density, i.e., $\{\mathcal{T}^{(\ell)}\}_{\#} \lambda \approx \varphi^{(\ell)}$, with a controlled error. This leads to a recursive construction procedure. Given $\mathcal{T}^{(\ell)}$, we need to add a new layer $\mathcal{Q}^{(\ell+1)}$ so that the new composition $\mathcal{T}^{(\ell+1)} = \mathcal{T}^{(\ell)} \circ \mathcal{Q}^{(\ell+1)}$ yields

$$\{\mathcal{T}^{(\ell)} \circ \mathcal{Q}^{(\ell+1)}\}_{\#} \lambda \approx \varphi^{(\ell+1)}.$$

This is equivalent to finding $\mathcal{Q}^{(\ell+1)}$ such that $\{\mathcal{Q}^{(\ell+1)}\}_{\#} \lambda \approx \{\mathcal{T}^{(\ell)}\}_{\#} \varphi^{(\ell+1)}$. Thus, we can build $\mathcal{Q}^{(\ell+1)}$ as a squared inverse Rosenblatt transport that pushes forward the reference density λ to the pullback density $\{\mathcal{T}^{(\ell)}\}_{\#} \varphi^{(\ell+1)}$. Since the pushforward of λ under $\mathcal{T}^{(\ell)}$ approximates $\varphi^{(\ell)}$, the pullback of the normalized density $\varphi^{(\ell)}$ under $\mathcal{T}^{(\ell)}$ satisfies

$$\{\mathcal{T}^{(\ell)}\}_{\#} \varphi^{(\ell)}(u) = \varphi^{(\ell)} \{ \mathcal{T}^{(\ell)}(u) | \nabla \mathcal{T}^{(\ell)}(u) \} \approx \lambda(u). \quad (18)$$

Similarly, we can see that

$$\{\mathcal{Q}^{(\ell+1)}\}_{\#} \lambda(u) \approx \{\mathcal{T}^{(\ell)}\}_{\#} \varphi^{(\ell+1)}(u) = \varphi^{(\ell+1)} \{ \mathcal{T}^{(\ell)}(u) | \nabla \mathcal{T}^{(\ell)}(u) \} \approx \frac{\varphi^{(\ell+1)} \{ \mathcal{T}^{(\ell)}(u) \}}{\varphi^{(\ell)} \{ \mathcal{T}^{(\ell)}(u) \}} \lambda(u).$$

With a suitable choice of bridging densities, the ratio $\varphi^{(\ell+1)}/\varphi^{(\ell)}$ is significantly less concentrated than the optimal importance density ρ^* . As a result, the map $\mathcal{Q}^{(\ell+1)}$ will be much easier to approximate than directly attempting to approximate the pullback of ρ^* to λ .

Although the normalizing constant of $\varphi^{(\ell+1)}$ is unknown, it is possible to recursively decompose the square root of the unnormalized pullback density $\{\mathcal{T}^{(\ell)}\}_{\#} \phi^{(\ell+1)}$ in tensor-train format using the construction outlined in Section 3.2. This procedure is summarized in Alg. 1.

Algorithm 1. Construction of deep importance density.

- Input: reference density λ and unnormalized bridging densities $\phi^{(1)}, \dots, \phi^{(L)}$
- Initialize the map as $\mathcal{T}^{(0)} \leftarrow I$ to have $\mathcal{T}^{(0)}(x) = x$.
- For $\ell = 1, \dots, L$, apply all steps as outlined in Section 3.2:
 - Factorize the square root of $\{\mathcal{T}^{(\ell-1)}\}_{\#} \phi^{(\ell)}(x)$ in a tensor-train format $\tilde{g}^{(\ell)}(x)$.
 - Choose appropriate $\tau^{(\ell)}$.
 - Construct the approximation $\{\mathcal{T}^{(\ell-1)}\}_{\#} \phi^{(\ell)}(x) \approx \rho^{(\ell)}(x) = \tilde{g}^{(\ell)}(x)^2 + \tau^{(\ell)} \lambda(x)$.
 - Compute the normalizing constant $\zeta^{(\ell)}$.
 - Compute the inverse Rosenblatt transport $\mathcal{Q}^{(\ell)}$ associated with $\rho^{(\ell)}$ as in (17).
 - Update the composition as $\mathcal{T}^{(\ell)} \leftarrow \mathcal{T}^{(\ell-1)} \circ \mathcal{Q}^{(\ell)}$.
- Return $\{\tilde{g}^{(\ell)}, \tau^{(\ell)}, \zeta^{(\ell)}\}_{\ell=1}^L$ and the composite map $\mathcal{T}^{(L)}$.

As shown in Appendix C, given the output of Alg. 1, the pushforward of the reference density λ under the composite map $\mathcal{T}^{(L)}$ has the normalized density $\bar{p} = \{\mathcal{T}^{(L)}\}_{\#} \lambda$ with

$$\bar{p}(x) = \left\{ \prod_{\ell=1}^L \zeta^{(\ell)} \right\}^{-1} \{ \tilde{g}^{(1)}(x)^2 + \tau^{(1)} \lambda(x) \} \prod_{\ell=2}^L \left(\frac{\tilde{g}^{(\ell)}[\{\mathcal{T}^{(\ell-1)}\}^{-1}(x)]^2}{\lambda[\{\mathcal{T}^{(\ell-1)}\}^{-1}(x)]} + \tau^{(\ell)} \right). \quad (19)$$

Since the Hellinger distance is invariant to a change of measure, our composite maps satisfy

$$D_{\text{H}} [\{\mathcal{T}^{(\ell-1)} \circ \mathcal{Q}^{(\ell)}\}_{\#} \lambda, \varphi^{(\ell)}] = D_{\text{H}} [\{\mathcal{Q}^{(\ell)}\}_{\#} \lambda, \{\mathcal{T}^{(\ell-1)}\}_{\#} \varphi^{(\ell)}],$$

for $1 \leq \ell \leq L$. As a consequence, the total Hellinger error of the approximate optimal importance density $\bar{p} = \{\mathcal{T}^{(L)}\}_{\#}\lambda$ is equivalent to the Hellinger error in the final iteration, $D_H[\{\mathcal{Q}^{(L)}\}_{\#}\lambda, \{\mathcal{T}^{(L-1)}\}_{\#}\varphi^{(L)}]$, which can be controlled by the L^2 -error of the tensor-train approximation, as shown in Lemma 1.

Under the assumption that the function of interest f is non-negative, the goal of deep importance sampling is to estimate the normalizing constant $\zeta^* = E_{\bar{p}}\{\rho^*(X)/\bar{p}(X)\}$. Using the change of variable $X = \mathcal{T}^{(L)}(U)$, where $X \sim \bar{p}$ and $U \sim \lambda$, the normalizing constant can be expressed equivalently as an expectation with respect to the reference density λ , such that

$$\zeta^* = E_{\lambda} \left[\frac{\rho^*\{\mathcal{T}(U)\}}{\bar{p}\{\mathcal{T}(U)\}} \right].$$

This leads to the *deep importance sampling estimator*

$$\hat{\zeta}_{\bar{p},N} = \frac{1}{N} \sum_{i=1}^N \frac{\rho^*\{\mathcal{T}^{(L)}(U^i)\}}{\bar{p}\{\mathcal{T}^{(L)}(U^i)\}}, \quad U^i \sim \lambda. \quad (20)$$

Its properties are established in the following lemma and the proof is given in [Appendix D](#).

LEMMA 2. *Suppose Assumptions 1–3 holds, and let $p^* = \rho^*/\zeta^*$ and \bar{p} be the exact optimal importance density and its approximation \bar{p} in (11) and (19), respectively.*

1. *Then $\text{supp}(p^*) \subseteq \text{supp}(\bar{p})$, $E_{\bar{p}}(\rho^*/\bar{p}) = \zeta^*$ and $\text{var}_{\bar{p}}(\rho^*/\bar{p}) < \infty$.*
2. *Assuming furthermore $\int \{\rho^*(x)/\pi_0(x)\}^3 \pi_0(x) dx < \infty$, then*

$$\text{var}_{\bar{p}}(p^*/\bar{p}) \leq C_p D_H(p^*, \bar{p}), \quad \text{where } C_p = 2 [E_{p^*}\{(p^*/\bar{p})^2\} - E_{\bar{p}}\{(p^*/\bar{p})^2\}]^{1/2}.$$

3. *Assuming instead that $\sup_{x \in \mathcal{X}} p^*(x)/\bar{p}(x) = M_{p^*, \bar{p}} < \infty$, then*

$$\text{var}_{\bar{p}}(p^*/\bar{p}) \leq C_m D_H(p^*, \bar{p})^2, \quad \text{where } C_m = 4 + 4M_{p^*, \bar{p}}.$$

The first condition of Lemma 2 establishes that the estimator $\hat{\zeta}_{\bar{p},N}$ is unbiased and satisfies the central limited theorem, i.e., $\sqrt{N}\hat{\zeta}_{\bar{p},N}$ converges in distribution to the normal distribution $\mathcal{N}\{\zeta^*, \text{var}_{\bar{p}}(\rho^*/\bar{p})\}$. Since $p^* = \rho^*/\zeta^*$, and thus $E_{\bar{p}}(p^*/\bar{p}) = 1$, the variance $\text{var}_{\bar{p}}(p^*/\bar{p})$ can be interpreted as the relative variance of the importance ratio ρ^*/\bar{p} , i.e., $(\zeta^*)^{-2} \text{var}_{\bar{p}}(\rho^*/\bar{p}) = \text{var}_{\bar{p}}(p^*/\bar{p})$. In this way, the relative mean square error of the estimator $\hat{\zeta}_{\bar{p},N}$ is given by

$$\text{rmse}(\hat{\zeta}_{\bar{p},N}, \zeta^*) = N^{-1} \{\zeta^*\}^{-2} \text{var}_{\bar{p}}(\rho^*/\bar{p}) = N^{-1} \text{var}_{\bar{p}}(p^*/\bar{p}).$$

Thus, to guarantee a $\text{rmse}(\hat{\zeta}_{\bar{p},N}, \zeta^*) \leq \varepsilon$ for some error threshold $\varepsilon > 0$, it is sufficient to choose either $N \geq C_p \varepsilon^{-1} D_H(p^*, \bar{p})$ or $N \geq C_m \varepsilon^{-1} D_H(p^*, \bar{p})^2$, depending on whether the assumption in Part 2 or Part 3 of Lemma 2 holds, respectively.

3.4. The ratio estimator: from a priori to a posteriori expectations

Finally, we want to extend the concept of deep importance sampling just introduced to the case of *a posteriori* expectations using the ratio estimator in (8). The optimal importance densities for estimating the numerator and the denominator in (8) are $p^* \propto f \mathcal{L}^y \pi_0$ and $q^* \propto \mathcal{L}^y \pi_0$, respectively. We can apply Alg. 1 to construct two composite maps $\mathcal{T}_p^{(L)}$ and $\mathcal{T}_q^{(L)}$ to approximately push forward the reference density λ to p^* and q^* , that is, $\{\mathcal{T}_p^{(L)}\}_{\#}\lambda = \bar{p} \approx p^*$, and $\{\mathcal{T}_q^{(L)}\}_{\#}\lambda = \bar{q} \approx q^*$. In fact, the optimal importance density for estimating the denominator Z is the normalized posterior, $q^* = \pi^y$. Thus, estimating the denominator here simply reduces to building a normalized posterior approximation. In general, we can choose different numbers of layers for $\mathcal{T}_p^{(L)}$ and $\mathcal{T}_q^{(L)}$ to adapt to the structures of two optimal densities.

We are now ready to define the *ratio estimator based on deep importance sampling*

$$\hat{R}_{\bar{p}, \bar{q}, N} = \frac{\hat{Q}_{\bar{p}, N}}{\hat{Z}_{\bar{q}, N}}, \quad \hat{Q}_{\bar{p}, N} = \frac{1}{N} \sum_{i=1}^N w_Q(U_p^i), \quad \hat{Z}_{\bar{q}, N} = \frac{1}{N} \sum_{i=1}^N w_Z(U_q^i), \quad U_p^i, U_q^i \sim \lambda, \quad (21)$$

where

$$w_Q(U) = \frac{f\{\mathcal{T}_p^{(L)}(U)\}\mathcal{L}^y\{\mathcal{T}_p^{(L)}(U)\}\pi_0\{\mathcal{T}_p^{(L)}(U)\}}{\bar{p}\{\mathcal{T}_p^{(L)}(U)\}}, \quad w_Z(U) = \frac{\mathcal{L}^y\{\mathcal{T}_q^{(L)}(U)\}\pi_0\{\mathcal{T}_q^{(L)}(U)\}}{\bar{q}\{\mathcal{T}_q^{(L)}(U)\}}.$$

For the purpose of variance reduction, we consider that each pair of random variables (U_p^i, U_q^i) follows some joint distribution but their marginal laws have the reference density λ .

To simplify notation, we define random variables $W_Q = w_Q(U_p)$ and $W_Z = w_Z(U_q)$. Under Assumptions 2 and 3, we have $E(W_Q) = Q$ and $E(W_Z) = Z$, and thus $\hat{Q}_{\bar{p},N}$ and $\hat{Z}_{\bar{q},N}$ are unbiased estimators of Q and Z , respectively. However, in general the resulting ratio estimator $\hat{R}_{\bar{p},\bar{q},N}$ is only asymptotically unbiased. In Lemmas 3 and 4, whose proofs are given in Appendix E, we want to characterize the asymptotic behaviour of the relative mean square error of $\hat{R}_{\bar{p},\bar{q},N}$ using its relative deviation from the *a posteriori* expectation, which is defined as

$$\Delta_{R,N} = \frac{\hat{R}_{\bar{p},\bar{q},N} - R}{R} = \frac{\sum_{i=1}^N W_Q^i / Q}{\sum_{i=1}^N W_Z^i / Z} - 1, \quad (22)$$

so that $\Delta_{R,N}$ is controlled by the laws of W_Q^1, \dots, W_Q^N and W_Z^1, \dots, W_Z^N .

LEMMA 3. *Suppose Assumptions 1–3 hold and the sequence $\{(W_Q^i, W_Z^i)\}_{i=1}^N$ is independent and identically distributed, but allowing each pair (W_Q^i, W_Z^i) to be correlated. Then, $\sqrt{N}\Delta_{R,N}$ converges in distribution to*

$$\mathcal{N}\left\{0, \frac{\text{var}(W_Q)}{Q^2} + \frac{\text{var}(W_Z)}{Z^2} - \frac{2\text{cov}(W_Q, W_Z)}{QZ}\right\}.$$

Thus, the ratio estimator in (21) is asymptotically unbiased and converges at the correct rate with respect to the sample size N . We also see that by correlating each pair of random variables (U_p^i, U_q^i) in (21) we can maximize the correlation between $W_Q = w_Q(U_p)$ and $W_Z = w_Z(U_q)$ to minimize the relative variance of the ratio estimator. For example, if λ is a zero mean Gaussian distribution, one can use the antithetic formula $U_p = aU_q + (1 - a^2)^{1/2}\epsilon$, with $\epsilon \sim \lambda$ and some constant a to correlate or anticorrelate the random variables. This way, the marginal distributions of (U_p, U_q) still have the same density λ , but U_p and U_q are correlated and it is possible to maximize $\text{cov}(W_Q, W_Z)$ as a function of a .

To get a more explicit, quantitative result regarding the benefits of the deep importance sampling strategy, in the following lemma we focus only on the case of independent samples U_p^i, U_q^i , for each $i = 1, \dots, N$.

LEMMA 4. *Under the assumptions of Lemma 3, but now assuming furthermore independence of the sequences $\{W_Q^i\}_{i=1}^N$ and $\{W_Z^i\}_{i=1}^N$ as well, the relative bias of $\hat{R}_{\bar{p},\bar{q},N}$ as $N \rightarrow \infty$ satisfies*

$$\frac{N|E(\hat{R}_{\bar{p},\bar{q},N}) - R|}{R} \rightarrow \frac{\text{var}(W_Z)}{Z^2},$$

and the relative mean square error of $\hat{R}_{\bar{p},\bar{q},N}$ satisfies

$$\text{rmse}(\hat{R}_{\bar{p},\bar{q},N}, R) = \mathcal{O}\left\{\frac{C_p D_H(p^*, \bar{p}) + C_q D_H(q^*, \bar{q})}{N} + \frac{1}{N^2}\right\}, \quad (23)$$

where $C_p = 2[E_{p^*}\{(p^*/\bar{p})^2\} - E_{\bar{p}}\{(p^*/\bar{p})^2\}]^{1/2}$ and $C_q = 2[E_{q^*}\{(q^*/\bar{q})^2\} - E_{\bar{q}}\{(q^*/\bar{q})^2\}]^{1/2}$.

Lemma 4 suggests that the bias is negligible with a large, finite sample size. Similar results for self-normalized importance sampling estimators have been shown in Theorem 2 of Li et al. (2013) under slightly stronger assumptions. More importantly, we see that the relative mean square error can be greatly reduced by constructing two importance densities \bar{p} and \bar{q} that can accurately approximate the corresponding optimal densities p^* and q^* . In theory, the Hellinger errors on the right hand side of (23) can be made to go to zero by increasing the tensor ranks and the number of discretization basis functions, leading to a zero-variance estimator. In comparison, the self-normalized importance sampling method uses identical

importance densities for estimating the numerator and the denominator, i.e., $\bar{p} = \bar{q}$, which is always sub-optimal at least for one of the terms and leads to a theoretical lower bound on the variance of the estimator for finite sample size that cannot be further reduced.

4. APPLICATION TO RARE EVENT ESTIMATION

As a challenging target application, we now use deep importance sampling to devise efficient estimators for *a priori* and *a posteriori* failure probabilities. The failure function $f(x) = \mathbf{1}_{\mathcal{A}}\{h(x)\}$ defined in (9) will in general have discontinuities at the boundary of the failure set $\mathcal{X}_F := \{x \in \mathcal{X} : f(x) = 1\}$. When the boundary of \mathcal{X}_F is not aligned with the coordinate axes in the parameter domain, the resulting tensor-train approximation of the optimal importance density may have high ranks. The discontinuities also make it challenging to choose appropriate bases to efficiently discretize the optimal importance density in each coordinate direction. To alleviate those difficulties and to provide a natural family of bridging densities $\phi^{(1)}, \dots, \phi^{(L)}$ for Alg. 1, we construct a smooth surrogate $g_\gamma(z; \mathcal{A})$ that converges to the indicator function $\mathbf{1}_{\mathcal{A}}(z)$ as $\gamma \rightarrow \infty$, that is, $g_\gamma(z; \mathcal{A})$ is continuous for $\gamma < \infty$ and $\lim_{\gamma \rightarrow \infty} g_\gamma(z; \mathcal{A}) = \mathbf{1}_{\mathcal{A}}(z)$.

For simplicity, we assume that $\mathcal{A} = [a, b]$ for some $a < b$. In fact, since the indicator function satisfies $\mathbf{1}_{[a,b]}(z) = \mathbf{1}_{[a,\infty)}(z) - \mathbf{1}_{(b,\infty)}(z)$ and $\mathbf{1}_{(-\infty,a]}(z) = 1 - \mathbf{1}_{(a,\infty)}(z)$ for any finite a and b , without loss of generality, it suffices to consider the case $\mathcal{A} = [a, \infty)$ with $a < \infty$. Since the weak derivative of $\mathbf{1}_{[a,\infty)}(z)$ is the Dirac delta $\delta(z - a)$, one can employ a probability density function $p_\gamma(z - a)$ such that $\lim_{\gamma \rightarrow \infty} p_\gamma(z - a)$ has the same distributional properties as $\delta(z - a)$, and then construct the surrogate function via the corresponding distribution function

$$g_\gamma(z; [a, \infty)) = \int_{-\infty}^z p_\gamma(z' - a) dz'.$$

In this work, we consider to use the density $p_\gamma(z - a) = [1 - \tanh\{(z - a)\gamma/2\}]^2 \gamma/4$, which leads to the *sigmoid function*

$$g_\gamma(z; [a, \infty)) = [1 + \exp\{\gamma(a - z)\}]^{-1}. \quad (24)$$

This defines a smoothed failure function

$$f_\gamma(x) = g_\gamma\{h(x); [a, \infty)\}.$$

Instead of directly approximating the optimal importance density $\rho^* = f\pi_0$ for estimating $E_{\pi_0}\{f(X)\}$, we choose a sufficiently large γ^* and approximate the smoothed version $f_{\gamma^*}\pi_0$ to avoid potential discontinuities. This smoothing strategy is also used in [Uribe et al. \(2021\)](#) for applying gradient-based dimension reduction methods in estimating *a priori* failure probability.

For the *a priori* rare event, we can now directly apply Alg. 1 to build a tensor-train approximation of $f_{\gamma^*}\pi_0$. The smoothed failure function $f_{\gamma^*}(x)$ may still have a large gradient near the boundary of the failure set \mathcal{X}_F and it can concentrate in the tail of π_0 . Thus, we use an increasing sequence of smoothing variables $\gamma_1 < \dots < \gamma_L = \gamma^*$ to define the unnormalized bridging densities

$$\phi^{(\ell)}(x) = f_{\gamma_\ell}(x)\pi_0(x), \quad \ell = 1, \dots, L,$$

for Alg. 1. The computed composite map $\mathcal{T}^{(L)}$ then provides an importance density $\bar{p} = \{\mathcal{T}^{(L)}\}_\# \lambda$ that is close to the smoothed optimal importance density $f_{\gamma^*}\pi_0$, and for γ^* sufficiently large, also close to the optimal importance density p^* . Finally, to estimate the *a priori* rare event probability, we can use the deep importance sampling estimator (20) with $\rho^* = f\pi_0$.

In [Appendix F](#), we make some heuristic observations that suggest that for sufficiently well-behaved $h(x)$ the Hellinger error induced by the smoothing may be $\mathcal{O}\{(\gamma^*)^{-1/2}\}$, providing some guidance for choosing γ^* to balance the smoothing error and the tensor-train approximation error. Moreover, we also provide a simple example in [Appendix G](#) to show that after smoothing, deep importance sampling does indeed work well on discontinuous densities that concentrate along a strongly nonlinear manifold.

To estimate the *a posteriori* rare event probability the ratio estimator based on deep importance sampling defined in (21) can be used. Using a tempering approach as in Gelman & Meng (1998) and Del Moral et al. (2006), the bridging densities for the denominator $E_{\pi_0}\{\mathcal{L}^y\}$ of the ratio estimator in Alg. 1 are chosen to be

$$\phi_d^{(\ell)}(x) = \{\mathcal{L}^y(x)\}^{\alpha_\ell} \pi_0(x), \quad 1 \leq \ell \leq L,$$

where $\alpha_1 < \dots < \alpha_L = 1$. For $\alpha_\ell \ll 1$, the unnormalized density $\{\mathcal{L}^y(x)\}^{\alpha_\ell} \pi_0(x)$ is significantly less concentrated compared to the unnormalized posterior $\mathcal{L}^y(x) \pi_0(x)$ and can be approximated more easily using tensor-trains. The resulting composite map $\mathcal{T}_q^{(L)}$ defines a density $\bar{q} = \{\mathcal{T}_q^{(L)}\}_\# \lambda$ that approximates the optimal importance density $q^* \equiv \pi^y$.

For the numerator $E_{\pi_0}\{f\mathcal{L}^y\}$ of the ratio estimator in (21), we smooth the failure function, as in the *a priori* case, and temper the likelihood to define bridging densities

$$\phi_n^{(\ell)}(x) = f_{\gamma_\ell}(x) \{\mathcal{L}^y(x)\}^{\beta_\ell} \pi_0(x), \quad 1 \leq \ell \leq L,$$

for Alg. 1, where $\gamma_1 < \dots < \gamma_L \equiv \gamma^*$ and $\beta_1 < \dots < \beta_L = 1$. This leads to the second composite map $\mathcal{T}_p^{(L)}$, which defines a density $\bar{p} = \{\mathcal{T}_p^{(L)}\}_\# \lambda$ that approximates the optimal importance density $p^* \propto f\mathcal{L}^y \pi_0$. Finally, the two importance densities \bar{p} and \bar{q} can be used in (21) to evaluate the ratio estimator for the *a posteriori* rare event probability.

5. EXAMPLE 1: SUSCEPTIBLE-INFECTIOUS-REMOVED MODEL

5.1. Problem setup

We consider a Bayesian parameter estimation problem for a compartmental susceptible-infectious-removed model, a simplified version of the model considered in Dutta et al. (2021). Given a spatially dependent demographic model consisting of $K \in \mathbb{N}$ compartments, we denote the numbers of susceptible, infectious and removed individuals in the k th compartment at a given time t by $S_k(t)$, $I_k(t)$ and $R_k(t)$, respectively. The interaction among the individuals within and across the different compartments is modelled by the following system of differential equations

$$\left. \begin{aligned} \frac{dS_k}{dt} &= -\theta_k S_k I_k + \frac{1}{2} \sum_{j \in \mathcal{J}_k} (S_j - S_k), \\ \frac{dI_k}{dt} &= \theta_k S_k I_k - \nu_k I_k + \frac{1}{2} \sum_{j \in \mathcal{J}_k} (I_j - I_k), \\ \frac{dR_k}{dt} &= \nu_k I_k + \frac{1}{2} \sum_{j \in \mathcal{J}_k} (R_j - R_k), \end{aligned} \right\} \quad (25)$$

where \mathcal{J}_k is the index set containing all neighbours of the k th compartment. See Fig. 1 for an example of the demographic connectivity graph of the states in Austria. The system of differential equations is parameterized by $\theta_k \in \mathbb{R}$ and $\nu_k \in \mathbb{R}$, representing the infection and recovery rate in the k th compartment, respectively. Our first aim is to estimate the unknown rate parameters $x = (\theta_1, \nu_1, \dots, \theta_K, \nu_K) \in \mathbb{R}^{2K}$ from noisy observations of $I_k(t)$ at discrete times. Then, we also aim to estimate the *a posteriori* risk, which is the probability of the number of infected individuals exceeding a chosen threshold.

5.2. Experiments on a one-dimensional lattice

We first consider a compartment model defined on a one-dimensional lattice, in which the k th compartment is only connected to compartments with adjacent indices $k - 1$ and $k + 1$. By changing the number of compartments, K , we can vary the parameter dimension to test the scalability of deep importance sampling. We impose periodic boundary conditions, such that $Z_{K+1} = Z_1$ and $Z_0 = Z_K$ for $Z \in \{S, I, R\}$. The differential equations in (25) are solved for the time interval $t \in [0, 5]$ with fixed inhomogeneous initial states $S_k(0) = 99 - K + k$, $I_k(0) = K + 1 - k$, and $R_k(0) = 0$ for $k = 1, \dots, K$.



Fig. 1: Compartment connectivity graph of the Austrian states.

For the Bayesian parameter estimation problem, synthetic observed data are generated from noisy measurements of infected population in each of compartments at 6 equidistant time points,

$$y_{k,j} = I_k \left(\frac{5j}{6}; x_{\text{true}} \right) + \eta_{k,j}, \quad \eta_{k,j} \sim \mathcal{N}(0, 1), \quad k = 1, \dots, K, \quad j = 1, \dots, 6,$$

where the “true” parameter $x_{\text{true}} = [0.1, 1, \dots, 0.1, 1]$, is used for simulating the synthetic observations. This leads to the likelihood function

$$\mathcal{L}^y(x) \propto \exp \left[-\frac{1}{2} \sum_{k=1}^K \sum_{j=1}^6 \left\{ I_k \left(\frac{5j}{6}; x \right) - y_{k,j} \right\}^2 \right]. \quad (26)$$

The differential equations are solved by the explicit Runge–Kutta method with adaptive time steps that control both absolute and relative errors to be within 10^{-6} . We specify a uniform prior on the domain $[0, 2]$ for each of θ_k and ν_k , which leads to $\pi_0(x) = \prod_{k=1}^{2K} \mathbf{1}_{[0,2]}(x_k)$. The *a posteriori* risk is defined as the posterior probability of the number of infected individuals in the last compartment at any time $t \in [0, 5]$ exceeding a threshold $I_{\max} > 0$,

$$\text{pr}_{\pi^y} \left\{ \max_{t \in [0,5]} I_K(t; X) > I_{\max} \right\}.$$

To apply deep importance sampling within the ratio estimator (21), we use a sequence of bridging densities $\phi_d^{(\ell)}(x) = \{\mathcal{L}^y(x)\}^{\alpha_\ell} \pi_0(x)$, $\ell = 1, \dots, L$, with tempered likelihood functions to guide Alg. 1 for the denominator. The tempering parameters start from $\alpha_1 = 10^{-4}$ and are incremented such that $\alpha_{\ell+1} = 10^{1/3} \alpha_\ell$ until $\alpha_L = 1$. Thus, $L = 13$. For the numerator of the ratio estimator (21), we use another sequence of bridging densities with the sigmoid smoothing

$$\phi_n^{(\ell)}(x) = \{\mathcal{L}^y(x)\}^{\beta_\ell} \pi_0(x) \left(1 + \exp \left[\gamma_\ell \left\{ I_{\max} - \max_{t \in [0,5]} I_K(t; x) \right\} \right] \right)^{-1}, \quad \ell = 1, \dots, L. \quad (27)$$

Here, we let $\beta_\ell = \alpha_\ell$. The smoothing widths are chosen such that $\gamma_\ell = \beta_\ell \gamma^*$, where γ^* will be varied in different experiments. In the construction of the tensor-train approximations, $\lambda(x)$ is a truncated normal reference distribution on $[-3, 3]$, and we use piecewise linear basis functions on a uniform grid with $n_k = n = 17$ points to discretize the densities in each coordinate direction.

Scalability and accuracy. We vary the number of compartments $K = \{3, 5, \dots, 15\}$ and take the threshold $I_{\max} = 88$. The threshold yields challenging values of the *a posteriori* risk below 10^{-6} for all numbers of compartments in this set of experiments. We use a sample size of $N = 2^{14}$ in the ratio estimator.

In the first experiment, we fix the tensor rank to $r_k = r = 7$ and the smoothing width to $\gamma^* = 10^4 / I_{\max}$. The Hellinger errors of the deep importance densities, the estimated *a posteriori* risks, and the number of density evaluations needed are shown in Fig. 2. We observe that the computational complexity, measured in the number of density evaluations, depends linearly on the dimension, while the Hellinger error increases only moderately for fixed tensor ranks, roughly logarithmically in the probability value itself.

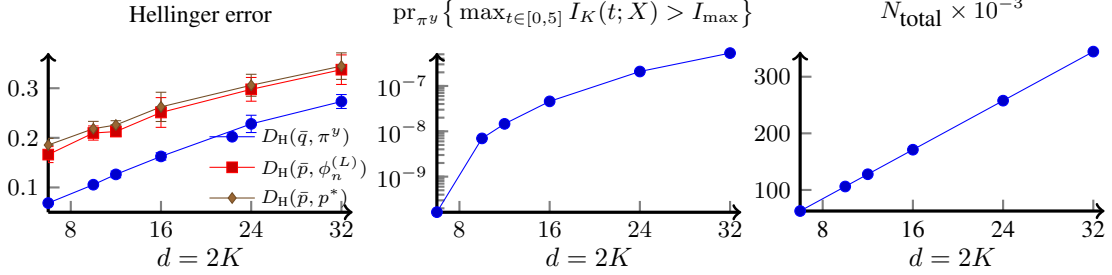


Fig. 2: Hellinger errors in the densities (left), estimated *a posteriori* risk (middle) and total number of function evaluations in Alg. 1 (right) for different numbers of compartments K in Example 1. In all figures, points denote average values, and error bars denote one standard deviation over 10 runs.

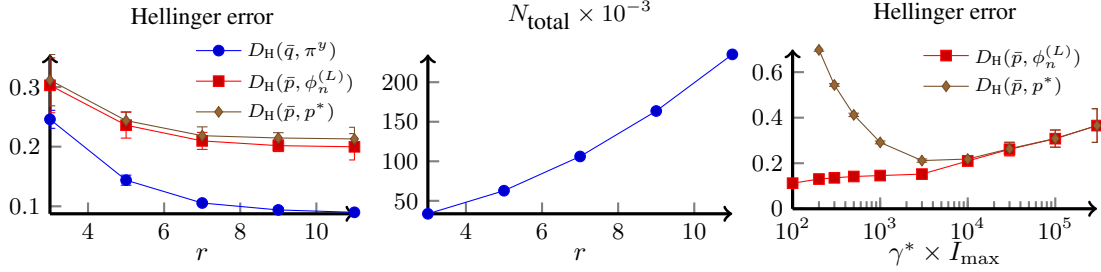


Fig. 3: Hellinger errors in the densities (left) and total number of function evaluations in Alg. 1 (middle) for different tensor ranks r , as well as Hellinger errors for different smoothing widths γ^* (right) in Example 1.

Then, we fix the number of compartments to $K = 5$, and investigate the impact of the tensor rank r and the smoothing width γ^* on the accuracy of deep importance sampling. Firstly, we set $\gamma^* = 10^4/I_{\max}$ and vary r . As shown in Fig. 3, the errors in all approximate densities decay with r until the discretization error is reached, whereas the number of function evaluations in Alg. 1 appears to depend quadratically on r . Secondly, we fix the tensor rank to $r = 7$ and vary the smoothing width γ^* . As shown in the right plot of Fig. 3, the error in approximating the smoothed optimal importance density depends monotonically on γ^* . This is expected, since a larger γ^* leads to a less smooth final biasing density $\phi_n^{(L)}(x)$ that is more difficult to approximate for Alg. 1. In contrast, the Hellinger distance of the approximation to the true optimal biasing density $p^*(x)$ grows strongly as γ^* decreases. The optimal value of γ^* is therefore an intermediate one, achieved for this example between $10^3/I_{\max}$ and $10^4/I_{\max}$.

Variance reduction via sample correlation. To confirm the variance reduction suggested by Lemma 3 we let $K = 5$, $I_{\max} = 88$, $\gamma^* = 3000/I_{\max}$ and $r = 7$. We consider positively correlated seed samples $U_p = U_q \sim \lambda$ with $a = 1$, uncorrelated samples $U_p \sim \lambda$ and $U_q \sim \lambda$ with $a = 0$, and negatively correlated samples with $a = -2/3$ and produce 20 batches of ratio estimators with $N = 2^{12}$ samples each. The relative standard deviations of the estimated *a posteriori* risk are $1.2e-2$, $1.4e-2$ and $2.4e-2$ for positively correlated, uncorrelated, and negatively correlated samples, respectively. Thus, the error is indeed reduced by making the correlation $\text{corr}(\Theta_Q, \Theta_Z) > 0$ positive, which confirms the result of Lemma 3.

Comparison with cross entropy. To benchmark our deep importance sampling approach we compare it to the cross entropy method of Botev & Kroese (2008). We vary the number of compartments, K , and compare the estimation accuracy of the cross entropy method and deep importance sampling. The cross entropy method has difficulties in estimating the rather small *a posteriori* risk in the above experiments. Therefore we reduce the threshold to $I_{\max} = 80$ in this experiment. For the cross entropy method, we use an importance density with a mixture of 4 Gaussian distributions. For our deep importance sampling method we use a tensor rank of $r = 7$ and a smoothing width of $\gamma^* = 3000/I_{\max}$. The estimated risks and

Table 1: Average value of the *a posteriori* risk in Example 1 over 10 runs, ± 1 standard deviation, using the cross entropy method and deep importance sampling.

K	Cross entropy		Deep importance sampling
	$N = 10^5$	$N = 10^6$	$N \approx 2 \cdot 10^4$
1	$4.4050\text{e-}5 \pm 1.56\text{e-}7$	$4.4165\text{e-}5 \pm 4.56\text{e-}8$	$4.4201\text{e-}5 \pm 1.65\text{e-}7$
2	$6.8283\text{e-}4 \pm 2.06\text{e-}3$	$7.3363\text{e-}5 \pm 4.01\text{e-}5$	$8.0586\text{e-}5 \pm 3.43\text{e-}7$
3	—	—	$3.3733\text{e-}4 \pm 1.10\text{e-}6$

their empirical standard deviations, which are computed over 10 replications, are summarized in Table 1. We observe that the accuracy of the cross entropy method deteriorates drastically with the dimension, making $K = 3$ compartments intractable even with a million samples per iteration. Increasing the number of mixture distributions gives similar results, while reducing it makes the results worse. In comparison, Alg. 1 is able to estimate the probability with less than 1% relative error in a fraction of the number of samples needed for the cross entropy method.

5.3. Experiments on the Austria model

Finally, we consider a more realistic setting where the model has $K = 9$ compartments following the Austrian state adjacency map shown in Fig. 1. The initial condition is given as $S_1(0) = 99$, $I_1(0) = 1$, $R_1(0) = 0$ (in Vorarlberg), and $S_k(0) = 100$, $I_k(0) = R_k(0) = 0$ elsewhere. We estimate parameters $x \in \mathbb{R}^{18}$ from synthetic noisy observation of $\{I_k(5j/12; x_{\text{true}})\}$, $k = 1, \dots, 9$, $j = 1, \dots, 12$, with the same “true” parameter and likelihood model specified in the first experiment. The risk is defined as the number of infected individuals in Burgenland, indexed by $k = 9$, at any time $t \in [0, 5]$ exceeding a threshold $I_{\max} = 69$. This value of I_{\max} corresponds to a dimensionless ratio of the highest number of hospitalizations (20000) and the expected initial number of infected individuals (290) employed in the modelling of lockdown strategies in England by Dutta et al. (2021).

To apply Alg. 1, we use the bridging densities defined above, with different starting tempering parameters $\alpha_1 = 10^{-5}$ and $L = 16$. The final smoothing width is fixed to $\gamma^* = 10^4/I_{\max}$. The tensor train ranks in each layer of Alg. 1 are adaptively chosen, with the maximum rank set to $r = 7$. To estimate the performance we use again 10 replicated experiments. The performance is as in the previous experiments. Both importance densities used in the ratio estimator can be accurately estimated using the layered transport maps. For the denominator and the numerator, the estimated Hellinger errors of the approximate importance densities are $D_{\text{H}}(\pi^y, \bar{q}) = 0.135 \pm 0.005$ and $D_{\text{H}}(p^*, \bar{p}) = 0.282 \pm 0.008$, respectively, using a total of 314371 ± 11727 density evaluations. The estimated *a posteriori* risk is 4.370×10^{-10} with estimated standard derivation 1.05×10^{-12} .

6. EXAMPLE 2: CONTAMINANT TRANSPORT IN GROUNDWATER

We aim to estimate the risk of contaminant transport in a steady-state groundwater system; see Cliffe et al. (2000) and the references therein. Here, the physical system is driven by some unknown random diffusivity field $\kappa(s, X)$ that cannot be directly observed, where $s \in D = [0, 1]^2$ is the spatial coordinate in the physical domain D and X , taking values in \mathbb{R}^d , is some parameter describing the randomness of the diffusivity. The observable state of the system is the water table $u(s, X)$, which is a function that satisfies the partial differential equation

$$-\nabla \cdot \{\kappa(s, X) \nabla u(s, X)\} = 0, \quad s \in (0, 1)^2, \quad (28)$$

with Dirichlet boundary conditions $u|_{s_1=0} = 1 + s_2/2$ and $u|_{s_1=1} = -\sin(2\pi s_2) - 1$ imposed horizontally and no-flux boundary conditions $\partial u/\partial s_2|_{s_2=0} = \partial u/\partial s_2|_{s_2=1} = 0$ imposed vertically. The Dirichlet boundary conditions generate an inhomogeneous horizontal Darcy flow field $\kappa(s, X) \nabla u(s, X)$. Figure 4 shows examples of flow fields and water tables generated by two different synthetic diffusivity fields.

Contaminant particles released at a fixed location $s^0 = (0, 0.5)$ on the left boundary are transported by the flow field according to the advection equation

$$\frac{ds(t, X)}{dt} = \kappa(s, X) \nabla u(s, X), \quad s(0, X) = s^0, \quad (29)$$

to arrive at the right boundary after some time τ . The particle paths are shown in the right column of Fig. 4. The risk in this scenario is defined as the probability, subject to the random diffusivity $\kappa(s, X)$, that the breakthrough time of contaminant particles, denoted by $\tau(X)$, is below some threshold τ_* .

We assign a log-normal prior to the spatial random field $\kappa(s, X)$. Using Karhunen-L oeve expansion the infinite-dimensional field $\log \kappa(s, X)$ with zero mean and a Gaussian covariance function with the correlation length $1/\sqrt{50}$ can be approximated by the finite representation

$$\log \kappa(s, X) = \sum_{k=1}^d X_k \sqrt{\lambda_k} \psi_k(s),$$

where each random coefficient X_k follows a standard normal prior $\mathcal{N}(0, 1)$ and $\{\psi_k(s), \lambda_k\}$ is the k th eigenpair of the associated covariance operator, in the descending order of the eigenvalues. For more details see Appendix H. A common practice in the engineering literature is to estimate the *a priori* risk by only considering the randomness induced by the prior distribution of $\kappa(s, X)$; see Peherstorfer et al. (2016); Uribe et al. (2021) and references therein for examples. As shown in Fig. 4, depending on the structure of the true diffusivity field, the contaminant breakthrough time can change due to localized changes that are difficult to detect. Thus, it is critical to also assess the *a posteriori* risk, where the uncertainty due to the unobserved diffusivity field $\kappa(s, X)$ can be better characterized by conditioning on the water table observed at a finite number of locations; see the black dots in the second column of Fig. 4 for the locations used in this example. The *a priori* risk and the *a posteriori* risk are given by $\text{pr}_{\pi_0} \{\tau(X) < \tau_*\}$ and $\text{pr}_{\pi_y} \{\tau(X) < \tau_*\}$, respectively. Each evaluation of $\tau(x)$ needs the numerical solution of the differential equations (28) and (29). Details of the numerical solvers and the likelihood function for the Bayesian parameter estimation are provided in Appendix H.

We first demonstrate the critical importance of computing the *a posteriori* risk rather than *a priori* risk in this example. We consider $d = 20$ components of the Karhunen-L oeve expansion, and a breakthrough time threshold $\tau_* = 0.1$. Without any observed data, the *a priori* risk computes to $6.3 \times 10^{-3} \pm 6.4 \times 10^{-4}$. Next, we generate the solution u from one of the ‘‘truth’’ coefficients depicted in Fig. 4 (left), and observe the solution at 15×15 equispaced spatial points with a zero-mean normal noise with variance 3×10^{-2} . Using the data generated from the diffusivity field with a low-diffusivity barrier in the top of Fig. 4, the *a posteriori* risk is $9.4 \times 10^{-4} \pm 1.3 \times 10^{-4}$. In comparison, using the data generated from the diffusivity field with a high-diffusivity channel in the bottom of Fig. 4, the *a posteriori* risk is $2.8 \times 10^{-2} \pm 0.2 \times 10^{-2}$, which is an order of magnitude higher. In addition, Fig. 5 shows cumulative density functions of the breakthrough time in the logarithmic scale. We observe that the law of breakthrough time significantly changes with observed data. In summary, the critical change of risk cannot be detected by computing the *a priori* risk in this example. Using observed data is essential to reliably estimate the risk of a groundwater system.

Additional numerical experiments with varying threshold τ_* , the smoothing width γ^* and the dimension d can be found in Appendix H. We provide there also numerical experiments on the estimation of the *a priori* risk, compared to the cross entropy method of Botev & Kroese (2008). In these experiments, deep importance sampling performs robustly with changing d and τ_* and achieves a nearly constant error versus dimension d . In comparison to the cross entropy method in the *a priori* case, the error is two orders of magnitude smaller, while using an order of magnitude fewer density evaluations.

7. FUTURE WORK

We demonstrated that on problems constrained by differential equations, our proposed deep importance sampling is able to compute hitherto unattainable estimates of rare event probabilities for complex, high-

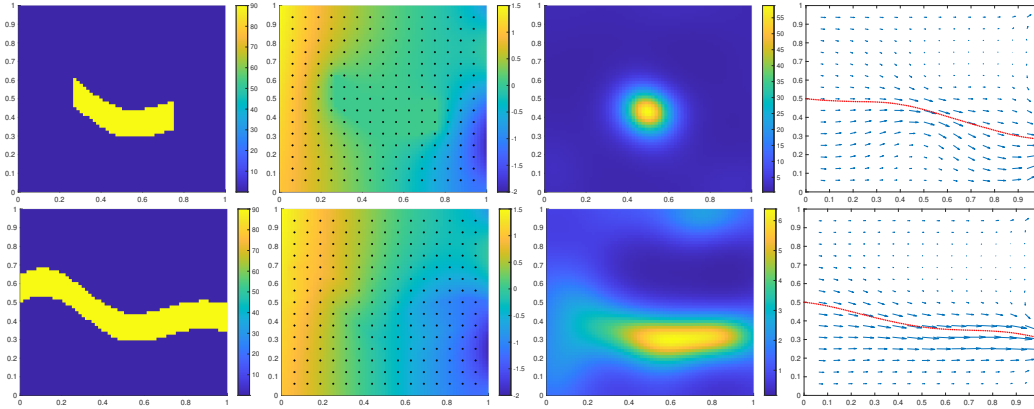


Fig. 4: Two groundwater experiments with a low diffusivity barrier (top row) and a high diffusivity channel (bottom row). First column: true diffusivity fields κ . Second column: water tables u generated by true κ with observation locations (black dots). Third column: maximum *a posteriori* estimates of diffusivity fields κ . Fourth column: flow fields (blue arrows) and particle trajectories (red) computed using κ in the third column. The maximum *a posteriori* particle breakthrough times of the top row and the bottom row are $\tau = 0.1886$ and $\tau = 0.0929$, respectively.

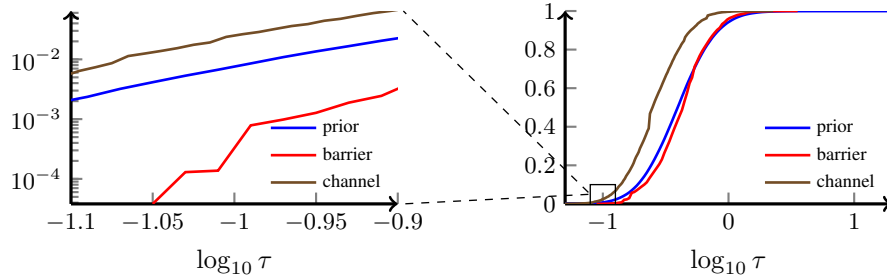


Fig. 5: Empirical cumulative density function of the breakthrough time, $\log_{10} \tau$, computed using 2^{17} samples from prior and posteriors conditional on two data sets shown in Figure 4. Left: zoom around the threshold $\tau_* = 0.1$.

dimensional posterior densities with $d > 20$. The approximation power of deep importance sampling can be further extended to problems with very high-dimensional parameters, e.g., $d > 10^3$, by combing it with gradient-based dimension reduction methods (Constantine et al., 2014; Cui et al., 2014; Cui & Tong, 2022; Zahm et al., 2022). Although deep importance sampling demonstrates a good statistical efficiency in terms of the effective sample size per function evaluation in our numerical experiments, the failure function can be computationally costly to evaluate due to the numerical solvers of the differential equations. This may prevent a reliable estimation of the failure probability with a limited computational budget. To address this bottleneck, our method can also be combined with either the multilevel Monte Carlo estimator (Elfverson et al., 2016; Scheichl et al., 2017; Wagner et al., 2020), or the multifidelity framework (Peherstorfer et al., 2016, 2018) in future research.

Acknowledgement. SD is thankful for the support from the Engineering and Physical Sciences Research Council New Investigator Award EP/T031255/1.

REFERENCES

- BIGONI, D., ENGSIG-KARUP, A. P. & MARZOUK, Y. M. (2016). Spectral tensor-train decomposition. *SIAM J. Sci. Comput.* **38**, A2405–A2439.
- BOTEV, Z. I. & KROESE, D. P. (2008). An efficient algorithm for rare-event probability estimation, combinatorial optimization, and counting. *Methodol. Comput. Appl. Probab.* **10**, 471–505.
- CAPPÉ, O., DOUC, R., GUILLIN, A., MARIN, J.-M. & ROBERT, C. P. (2008). Adaptive importance sampling in general mixture classes. *Stat. Comput.* **18**, 447–459.
- CLIFFE, K. A., GRAHAM, I. G., SCHEICHL, R. & STALS, L. (2000). Parallel computation of flow in heterogeneous media modelled by mixed finite elements. *J. Comput. Phys.* **164**, 258–282.
- CONSTANTINE, P. G., DOW, E. & WANG, Q. (2014). Active subspace methods in theory and practice: Applications to kriging surfaces. *SIAM J. Sci. Comput.* **36**, A1500–A1524.
- CORNUET, J.-M., MARIN, J.-M., MIRA, A. & ROBERT, C. P. (2012). Adaptive multiple importance sampling. *Scand. J. Stat.* **39**, 798–812.
- CUI, T. & DOLGOV, S. (2021). Deep composition of tensor-trains using squared inverse rosenblatt transports. *Found. Comput. Math.*, in press.
- CUI, T., MARTIN, J., MARZOUK, Y. M., SOLONEN, A. & SPANTINI, A. (2014). Likelihood-informed dimension reduction for nonlinear inverse problems. *Inverse Probl.* **30**, 114015.
- CUI, T. & TONG, X. T. (2022). A unified performance analysis of likelihood-informed subspace methods. *Bernoulli*, **28**, 2788–2815.
- DEL MORAL, P., DOUCET, A. & JASRA, A. (2006). Sequential monte carlo samplers. *J. R. Stat. Soc. Series B Stat. Methodol.* **68**, 411–436.
- DODWELL, T. J., KYNASTON, S., BUTLER, R., HAFTKA, R. T., KIM, N. H. & SCHEICHL, R. (2021). Multilevel monte carlo simulations of composite structures with uncertain manufacturing defects. *Probabilistic Eng. Mech.* **63**, 103116.
- DOLGOV, S., ANAYA-IZQUIERDO, K., FOX, C. & SCHEICHL, R. (2020). Approximation and sampling of multivariate probability distributions in the tensor train decomposition. *Stat. Comput.* **30**, 603–625.
- DOLGOV, S. V. & SAVOSTYANOV, D. V. (2014). Alternating minimal energy methods for linear systems in higher dimensions. *SIAM J. Sci. Comput.* **36**, A2248–A2271.
- DOUC, R., GUILLIN, A., MARIN, J.-M. & ROBERT, C. P. (2007). Convergence of adaptive mixtures of importance sampling schemes. *Ann. Stat.* **35**, 420–448.
- DUTTA, R., GOMES, S. N., KALISE, D. & PACCHIARDI, L. (2021). Using mobility data in the design of optimal lockdown strategies for the COVID-19 pandemic. *PLoS Comput. Biol.* **17**, 1–25.
- ELFVÉRSO, D., HELLMAN, F. & MÅLQVIST, A. (2016). A multilevel monte carlo method for computing failure probabilities. *SIAM/ASA J. Uncertain. Quantif.* **4**, 312–330.
- GELMAN, A. & MENG, X.-L. (1998). Simulating normalizing constants: From importance sampling to bridge sampling to path sampling. *Stat. Sci.*, 163–185.
- GORODETSKY, A., KARAMAN, S. & MARZOUK, Y. M. (2019). A continuous analogue of the tensor-train decomposition. *Comput. Methods Appl. Mech. Eng.* **347**, 59–84.
- GRIEBEL, M. & HARBRECHT, H. (2021). Analysis of tensor approximation schemes for continuous functions. *Found. Comput. Math.*, in press.
- HACKBUSCH, W. (2012). *Tensor spaces and numerical tensor calculus*, vol. 42. Springer Science & Business Media.
- JOHNSON, M. (1987). *Multivariate Statistical Simulation*. New York: Wiley.
- LI, W., TAN, Z. & CHEN, R. (2013). Two-stage importance sampling with mixture proposals. *J. Am. Stat. Assoc.* **108**, 1350–1365.
- OH, M.-S. & BERGER, J. O. (1993). Integration of multimodal functions by monte carlo importance sampling. *J. Am. Stat. Assoc.* **88**, 450–456.
- OSELEDETS, I. & TYRTYSHNIKOV, E. (2010). TT-cross approximation for multidimensional arrays. *Linear Algebra Appl.* **432**, 70–88.
- OSELEDETS, I. V. (2011). Tensor-train decomposition. *SIAM J. Sci. Comput.* **33**, 2295–2317.
- PEHERSTORFER, B., CUI, T., MARZOUK, Y. & WILLCOX, K. (2016). Multifidelity importance sampling. *Comput. Methods Appl. Mech. Eng.* **300**, 490–509.
- PEHERSTORFER, B., KRAMER, B. & WILLCOX, K. (2018). Multifidelity preconditioning of the cross-entropy method for rare event simulation and failure probability estimation. *SIAM/ASA J. Uncertain. Quantif.* **6**, 737–761.
- ROHRBACH, P. B., DOLGOV, S., GRASEDYCK, L. & SCHEICHL, R. (2022). Rank bounds for approximating Gaussian densities in the Tensor-Train format. *SIAM/ASA J. Uncertain. Quantif.*, in press.
- ROSENBLATT, M. (1952). Remarks on a multivariate transformation. *Ann. Math. Stat.* **23**, 470–472.
- SCHEICHL, R., STUART, A. M. & TECKENTRUP, A. L. (2017). Quasi-Monte Carlo and Multilevel Monte Carlo methods for computing posterior expectations in elliptic inverse problems. *SIAM/ASA J. Uncertain. Quantif.* **5**, 493–518.
- URIBE, F., PAPAIOANNOU, I., MARZOUK, Y. M. & STRAUB, D. (2021). Cross-entropy-based importance sampling with failure-informed dimension reduction for rare event simulation. *SIAM/ASA J. Uncertain. Quantif.* **9**, 818–847.

- WAGNER, F., LATZ, J., PAPAIOANNOU, I. & ULLMANN, E. (2020). Multilevel sequential importance sampling for rare event estimation. *SIAM J. Sci. Comput.* **42**, A2062–A2087.
- ZAHM, O., CUI, T., LAW, K., SPANTINI, A. & MARZOUK, Y. (2022). Certified dimension reduction in nonlinear bayesian inverse problems. *Math. Comput.*, **91**, 1789–1835.

APPENDIX A. PROOF OF LEMMA 1

LEMMA 1. Suppose $\|\sqrt{\rho^*} - \tilde{g}\|_2 \leq \epsilon$ and $\tau \leq \epsilon^2$. Then, the exact normalizing constant ζ^* in (11) and its approximation ζ in (13) satisfy $|\zeta^* - \zeta| \leq \sqrt{2}\epsilon$ and the Hellinger distance between p^* and its normalized approximation p defined in (13) can be bounded by $D_H(p^*, p) \leq 2\epsilon/\sqrt{\zeta^*}$.

Proof. Recall that the unnormalized optimal importance density ρ^* is approximated by $\rho = \tilde{g}^2 + \tau\lambda$, where λ is a normalized probability density, $\tau > 0$, and \tilde{g} satisfies $\|\sqrt{\rho^*} - \tilde{g}\|_2 \leq \epsilon$. Since ρ^* and λ are non-negative functions and $\tau > 0$, we have the identity

$$\begin{aligned} (\sqrt{\rho^*} - \sqrt{\rho})^2 &= \{\sqrt{\rho^*} - (\tilde{g}^2 + \tau\lambda)^{1/2}\}^2 \\ &= \rho^* + \tilde{g}^2 + \tau\lambda - 2\sqrt{\rho^*}(\tilde{g}^2 + \tau\lambda)^{1/2} \\ &\leq \rho^* + \tilde{g}^2 + \tau\lambda - 2\sqrt{\rho^*}\tilde{g} \\ &= (\sqrt{\rho^*} - \tilde{g})^2 + \tau\lambda, \end{aligned}$$

which leads to $\|\sqrt{\rho^*} - \sqrt{\rho}\|_2^2 \leq \|\sqrt{\rho^*} - \tilde{g}\|_2^2 + \tau \leq \epsilon^2 + \tau$. Choosing $\tau \leq \epsilon^2$, we have

$$\|\sqrt{\rho^*} - \sqrt{\rho}\|_2 \leq \sqrt{2}\epsilon. \quad (\text{A.1})$$

Since the square roots of the normalising constants can be expressed as $\sqrt{\zeta^*} = \|\sqrt{\rho^*}\|_2$ and $\sqrt{\zeta} = \|\sqrt{\rho}\|_2$, we have

$$\begin{aligned} |\sqrt{\zeta^*} - \sqrt{\zeta}|(\sqrt{\zeta^*} + \sqrt{\zeta}) &= |\zeta^* - \zeta| \\ &= \left| \int_{\mathcal{X}} \rho^*(x) - \rho(x) dx \right| \\ &= |\langle \sqrt{\rho^*} - \sqrt{\rho}, \sqrt{\rho^*} + \sqrt{\rho} \rangle| \\ &\leq \|\sqrt{\rho^*} - \sqrt{\rho}\|_2 \|\sqrt{\rho^*} + \sqrt{\rho}\|_2 \\ &\leq \|\sqrt{\rho^*} - \sqrt{\rho}\|_2 (\|\sqrt{\rho^*}\|_2 + \|\sqrt{\rho}\|_2) \\ &= \|\sqrt{\rho^*} - \sqrt{\rho}\|_2 (\sqrt{\zeta^*} + \sqrt{\zeta}). \end{aligned}$$

This leads to

$$|\sqrt{\zeta^*} - \sqrt{\zeta}| \leq \|\sqrt{\rho^*} - \sqrt{\rho}\|_2. \quad (\text{A.2})$$

Thus, the result of the first property of Lemma 1 follows.

Recall that the Hellinger distance is proportional to the L^2 distance of the normalized densities, i.e.,

$$D_H(p^*, p) = \left[\frac{1}{2} \int \{\sqrt{p^*}(x) - \sqrt{p}(x)\}^2 dx \right]^{\frac{1}{2}} = \frac{1}{\sqrt{2}} \|\sqrt{p^*} - \sqrt{p}\|_2.$$

The L^2 distance of the normalized densities follows the identity

$$\begin{aligned} \|\sqrt{p^*} - \sqrt{p}\|_2 &= \left\| \frac{\sqrt{\rho^*}}{\sqrt{\zeta^*}} - \frac{\sqrt{\rho}}{\sqrt{\zeta}} \right\|_2 = \frac{1}{\sqrt{\zeta^*}} \left\| \sqrt{\rho^*} - \sqrt{\rho} + \sqrt{\rho} - \sqrt{\rho} \frac{\sqrt{\zeta^*}}{\sqrt{\zeta}} \right\|_2 \\ &\leq \frac{1}{\sqrt{\zeta^*}} \|\sqrt{\rho^*} - \sqrt{\rho}\|_2 + \frac{1}{\sqrt{\zeta^*}} \left\| \sqrt{\rho} \left(1 - \frac{\sqrt{\zeta^*}}{\sqrt{\zeta}} \right) \right\|_2 \\ &= \frac{1}{\sqrt{\zeta^*}} \|\sqrt{\rho^*} - \sqrt{\rho}\|_2 + \frac{\sqrt{\zeta}}{\sqrt{\zeta^*}} \left(1 - \frac{\sqrt{\zeta^*}}{\sqrt{\zeta}} \right) \\ &= \frac{1}{\sqrt{\zeta^*}} (\|\sqrt{\rho^*} - \sqrt{\rho}\|_2 + \sqrt{\zeta} - \sqrt{\zeta^*}) \\ &\leq \frac{2}{\sqrt{\zeta^*}} \|\sqrt{\rho^*} - \sqrt{\rho}\|_2, \end{aligned}$$

where the last inequality follows from (A.2). Substituting (A.1) into the above inequality and the definition of the Hellinger distance, we obtain $D_H(p^*, p) \leq 2\epsilon/\sqrt{\zeta^*}$. This gives the second property. \square

APPENDIX B. MARGINALISATION

To realize the map \mathcal{Q} , our starting point is to construct a sequence of unnormalized marginal densities

$$\rho_{\leq k}(x_{\leq k}) = \int_{\mathcal{X}_{>k}} \rho(x_{\leq k}, x_{>k}) dx_{>k} = \int_{\mathcal{X}_{>k}} \tilde{g}(x_{\leq k}, x_{>k})^2 dx_{>k} + \tau \lambda_{\leq k}(x_{\leq k}), \quad (\text{B.1})$$

where $\lambda_{\leq k}(x_{\leq k}) = \prod_{j=1}^k \lambda_j(x_j)$, for all $1 \leq k < d$. Recalling the tensor-train decomposition

$$\tilde{g}(x) = \mathbf{G}_1(x_1) \cdots \mathbf{G}_k(x_k) \cdots \mathbf{G}_d(x_d),$$

we can define

$$\mathbf{G}_{\leq k}(x_{\leq k}) = \mathbf{G}_1(x_1) \cdots \mathbf{G}_k(x_k), \quad \mathbf{G}_{>k}(x_{>k}) = \mathbf{G}_{k+1}(x_{k+1}) \cdots \mathbf{G}_d(x_d),$$

where $\mathbf{G}_{\leq k}(x_{\leq k}) \in \mathbb{R}^{1 \times r_k}$ and $\mathbf{G}_{>k}(x_{>k}) \in \mathbb{R}^{r_k \times 1}$ are row-vector-valued and column-vector-valued functions, respectively. Then, \tilde{g} can be written as $\tilde{g}(x_{\leq k}, x_{>k}) = \mathbf{G}_{\leq k}(x_{\leq k}) \mathbf{G}_{>k}(x_{>k})$. The integration of \tilde{g}^2 over $x_{>k}$ for any index k , and hence the unnormalized marginal densities, can be obtained dimension-by-dimension as follows.

1. For $k = d - 1$, we integrate \tilde{g}^2 over the last coordinate x_d to obtain

$$\begin{aligned} \rho_{<d}(x_{<d}) &= \int_{\mathcal{X}_d} \left\{ \sum_{\alpha_{d-1}=1}^{r_{d-1}} \mathbf{G}_{<d}^{(\alpha_{d-1})}(x_{<d}) \mathbf{G}_d^{(\alpha_{d-1})}(x_d) \right\}^2 dx_d + \tau \lambda_{<d}(x_{<d}) \\ &= \sum_{\alpha_{d-1}=1}^{r_{d-1}} \sum_{\beta_{d-1}=1}^{r_{d-1}} \mathbf{G}_{<d}^{(\alpha_{d-1})}(x_{<d}) \mathbf{G}_{<d}^{(\beta_{d-1})}(x_{<d}) \mathbf{M}_d^{(\alpha_{d-1}, \beta_{d-1})} + \tau \lambda_{<d}(x_{<d}), \end{aligned}$$

where $\mathbf{M}_d \in \mathbb{R}^{r_{d-1} \times r_{d-1}}$ is a symmetric positive definite mass matrix such that

$$\mathbf{M}_d^{(\alpha_{d-1}, \beta_{d-1})} = \int_{\mathcal{X}_d} \mathbf{G}_d^{(\alpha_{d-1})}(x_d) \mathbf{G}_d^{(\beta_{d-1})}(x_d) dx_d. \quad (\text{B.2})$$

Computing the Cholesky factorization $\mathbf{L}_d \mathbf{L}_d^\top = \mathbf{M}_d$, we have the simplification

$$\rho_{<d}(x_{<d}) = \sum_{\alpha_{d-1}=1}^{r_{d-1}} \left\{ \mathbf{G}_{<d}(x_{<d}) \mathbf{L}_d^{(:, \alpha_{d-1})} \right\}^2 + \tau \lambda_{<d}(x_{<d}). \quad (\text{B.3})$$

2. For any index $1 < k < d$, suppose we have the symmetric positive definite mass matrix $\bar{\mathbf{M}}_{>k} \in \mathbb{R}^{r_k \times r_k}$ such that

$$\bar{\mathbf{M}}_{>k}^{(\alpha_k, \beta_k)} = \int_{\mathcal{X}_{>k}} \mathbf{G}_{>k}^{(\alpha_k)}(x_d) \mathbf{G}_{>k}^{(\beta_k)}(x_{>k}) dx_{>k}$$

and its Cholesky factorization $\bar{\mathbf{L}}_{>k} \bar{\mathbf{L}}_{>k}^\top = \bar{\mathbf{M}}_{>k}$. Then, similar to the above case, we have the unnormalized marginal density

$$\rho_{\leq k}(x_{\leq k}) = \sum_{\alpha_k=1}^{r_k} \left\{ \mathbf{G}_{\leq k}(x_{\leq k}) \bar{\mathbf{L}}_{>k}^{(:, \alpha_k)} \right\}^2 + \tau \lambda_{\leq k}(x_{\leq k}).$$

This way, the next unnormalized marginal density $\rho_{<k}(x_{<k})$ can be constructed by a one-dimensional integration over x_k , which takes the form

$$\begin{aligned} \rho_{<k}(x_{<k}) &= \sum_{\alpha_{k-1}=1}^{r_{k-1}} \int_{\mathcal{X}_k} \left\{ \sum_{\alpha_{k-1}=1}^{r_{k-1}} \mathbf{G}_{<k}^{(\alpha_{k-1})}(x_{<k}) \mathbf{G}_k^{(\alpha_{k-1}, :)}(x_k) \bar{\mathbf{L}}_{>k}^{(:, \alpha_k)} \right\}^2 dx_k + \tau \lambda_{<k}(x_{<k}) \\ &= \sum_{\alpha_{k-1}=1}^{r_{k-1}} \sum_{\beta_{k-1}=1}^{r_{k-1}} \mathbf{G}_{<k}^{(\alpha_{k-1})}(x_{<k}) \mathbf{G}_{<k}^{(\beta_{k-1})}(x_{<k}) \bar{\mathbf{M}}_{\geq k}^{(\alpha_{k-1}, \beta_{k-1})} + \tau \lambda_{<k}(x_{<k}), \end{aligned}$$

where $\bar{M}_{\geq k} \in \mathbb{R}^{r_{k-1} \times r_{k-1}}$ is the next mass matrix such that

$$\bar{M}_{\geq k}^{(\alpha_{k-1}, \beta_{k-1})} = \sum_{\alpha_k=1}^{r_k} \int_{\mathcal{X}_k} \{G_k^{(\alpha_{k-1}, \cdot)}(x_k) \bar{L}_{>k}^{(\cdot, \alpha_k)}\} \{G_k^{(\beta_{k-1}, \cdot)}(x_k) \bar{L}_{>k}^{(\cdot, \alpha_k)}\} dx_k. \quad (\text{B.4})$$

Again, by computing the Cholesky factorization $\bar{L}_{\geq k} \bar{L}_{\geq k}^\top = \bar{M}_{\geq k}$, we have the simplified marginal density

$$\rho_{<k}(x_{<k}) = \sum_{\alpha_{k-1}=1}^{r_{k-1}} \left\{ G_{<k}(x_{<k}) \bar{L}_{\geq k}^{(\cdot, \alpha_{k-1})} \right\}^2 + \tau \lambda_{<k}(x_{<k}). \quad (\text{B.5})$$

Following the above procedure, initializing $\bar{M}_{>k}$ with $\bar{M}_{>k} = M_d$ for $k = d - 1$, we can recursively construct all unnormalized marginal densities. In each iteration, we only need to solve a one-dimensional integration problem in (B.4). Given n_k number of discretization basis functions in x_k , the total computational complexity of solving the integration in (B.4) and computing the Cholesky factorization $\bar{L}_{\geq k}$ is $\mathcal{O}(n_k r_k r_{k-1}^2 + r_{k-1}^3)$.

3. For $k = 1$, we have the unnormalized marginal density

$$\rho_{\leq 1}(x_1) = \sum_{\alpha_1=1}^{r_1} \left\{ G_1(x_1) \bar{L}_{>1}^{(\cdot, \alpha_1)} \right\}^2 + \tau \lambda_{\leq 1}(x_1).$$

Carrying out one extra integration defined in (B.4), we obtain $\bar{M}_{\geq 1} \in \mathbb{R}$ as $r_0 = 1$. This gives the normalising constant $\zeta = \bar{M}_{\geq 1} + \tau$.

APPENDIX C. PUSHFORWARD DENSITY OF THE COMPOSITE MAP

As a starting point, we derive the Jacobian of the incremental map $u' = \mathcal{Q}^{(\ell)}(u)$, which has the form

$$\mathcal{Q}^{(\ell)} = \mathcal{F}^{-1} \circ \mathcal{R},$$

with $\mathcal{F}_\# p^{(\ell)} = \mu$ and $\mathcal{R}_\# \lambda = \mu$, where μ is the uniform density on $[0, 1]^d$ and

$$p^{(\ell)}(u') = \frac{1}{\zeta^{(\ell)}} \left\{ \tilde{g}^{(\ell)}(u')^2 + \tau^{(\ell)} \lambda(u') \right\} \quad (\text{C.1})$$

is the ℓ -th approximate density. Thus, we have the identity

$$p^{(\ell)}(u') = \{\mathcal{Q}^{(\ell)}\}_\# \lambda(u') = \lambda \left[\{\mathcal{Q}^{(\ell)}\}^{-1}(u') \right] |\nabla \{\mathcal{Q}^{(\ell)}\}^{-1}(u')|, \quad (\text{C.2})$$

which gives the Jacobian

$$|\nabla \{\mathcal{Q}^{(\ell)}\}^{-1}(u')| = \frac{p^{(\ell)}(u')}{\lambda \left[\{\mathcal{Q}^{(\ell)}\}^{-1}(u') \right]}.$$

Given a composite map $\mathcal{T}^{(\ell)} = \mathcal{T}^{(\ell-1)} \circ \mathcal{Q}^{(\ell)}$, to avoid confusion, we define the associated change of variables as

$$x = \mathcal{T}^{(\ell)}(u) \iff u' = \mathcal{Q}^{(\ell)}(u), \quad x = \mathcal{T}^{(\ell-1)}(u'),$$

and the reverse transform as

$$u = \{\mathcal{T}^{(\ell)}\}^{-1}(x) \iff u' = \{\mathcal{T}^{(\ell-1)}\}^{-1}(x), \quad u = \{\mathcal{Q}^{(\ell)}\}^{-1}(u').$$

This way, the Jacobian of the inverse map satisfies

$$|\nabla \{\mathcal{T}^{(\ell)}\}^{-1}(x)| = |\nabla \{\mathcal{Q}^{(\ell)}\}^{-1}(u')| |\nabla \{\mathcal{T}^{(\ell-1)}\}^{-1}(x)|,$$

by the chain rule. Substituting (C.2) and $u' = \{\mathcal{T}^{(\ell-1)}\}^{-1}(x)$ into the above identity, the Jacobian of the composite map satisfies the recurrence relationship

$$\begin{aligned} |\nabla\{\mathcal{T}^{(\ell)}\}^{-1}(x)| &= |\nabla\{\mathcal{T}^{(\ell-1)}\}^{-1}(x)| \frac{p^{(\ell)}[\{\mathcal{T}^{(\ell-1)}\}^{-1}(x)]}{\lambda(\{\mathcal{Q}^{(\ell)}\}^{-1}[\{\mathcal{T}^{(\ell-1)}\}^{-1}(x)])} \\ &= |\nabla\{\mathcal{T}^{(\ell-1)}\}^{-1}(x)| \frac{p^{(\ell)}[\{\mathcal{T}^{(\ell-1)}\}^{-1}(x)]}{\lambda[\{\mathcal{T}^{(\ell)}\}^{-1}(x)]} \end{aligned} \quad (\text{C.3})$$

Thus, by induction, the Jacobian of the composite of L layers of maps, $\mathcal{T}^{(L)}$, satisfies

$$\begin{aligned} |\nabla\{\mathcal{T}^{(L)}\}^{-1}(x)| &= |\nabla\{\mathcal{T}^{(0)}\}^{-1}(x)| \left(\frac{p^{(1)}[\{\mathcal{T}^{(0)}\}^{-1}(x)]}{\lambda[\{\mathcal{T}^{(1)}\}^{-1}(x)]} \dots \frac{p^{(L)}[\{\mathcal{T}^{(L-1)}\}^{-1}(x)]}{\lambda[\{\mathcal{T}^{(L)}\}^{-1}(x)]} \right) \\ &= \frac{p^{(1)}(x)}{\lambda[\{\mathcal{T}^{(L)}\}^{-1}(x)]} \prod_{\ell=2}^L \frac{p^{(\ell)}[\{\mathcal{T}^{(\ell-1)}\}^{-1}(x)]}{\lambda[\{\mathcal{T}^{(\ell-1)}\}^{-1}(x)]}. \end{aligned} \quad (\text{C.4})$$

Substituting (C.4) into the identity

$$\{\mathcal{T}^{(L)}\}_{\#} \lambda(x) = \lambda[\{\mathcal{T}^{(L)}\}^{-1}(x)] |\nabla\{\mathcal{T}^{(L)}\}^{-1}(x)|$$

and applying (C.1), the pushforward density of λ under $\mathcal{T}^{(L)}$ has the density

$$\begin{aligned} \{\mathcal{T}^{(L)}\}_{\#} \lambda(x) &= p^{(1)}(x) \prod_{\ell=2}^L \frac{p^{(\ell)}[\{\mathcal{T}^{(\ell-1)}\}^{-1}(x)]}{\lambda[\{\mathcal{T}^{(\ell-1)}\}^{-1}(x)]} \\ &= \left\{ \prod_{\ell=1}^L \zeta^{(\ell)} \right\}^{-1} \{ \tilde{g}^{(1)}(x)^2 + \tau^{(1)}\lambda(x) \} \prod_{\ell=2}^L \left(\frac{\tilde{g}^{(\ell)}[\{\mathcal{T}^{(\ell-1)}\}^{-1}(x)]^2}{\lambda[\{\mathcal{T}^{(\ell-1)}\}^{-1}(x)]} + \tau^{(\ell)} \right). \end{aligned} \quad (\text{C.5})$$

This concludes the derivation. \square

APPENDIX D. PROOF OF LEMMA 2

LEMMA 2. *Suppose Assumptions 1–3 holds, and let $p^* = \rho^*/\zeta^*$ and \bar{p} be the exact optimal importance density and its approximation \bar{p} in (11) and (19), respectively.*

1. *Then $\text{supp}(p^*) \subseteq \text{supp}(\bar{p})$, $E_{\bar{p}}(\rho^*/\bar{p}) = \zeta^*$ and $\text{var}_{\bar{p}}(\rho^*/\bar{p}) < \infty$.*
2. *Assuming furthermore $\int \{\rho^*(x)/\pi_0(x)\}^3 \pi_0(x) dx < \infty$, then*

$$\text{var}_{\bar{p}}(p^*/\bar{p}) \leq C_p D_H(p^*, \bar{p}), \quad \text{where } C_p = 2 [E_{p^*}\{(p^*/\bar{p})^2\} - E_{\bar{p}}\{(p^*/\bar{p})^2\}]^{1/2}.$$

3. *Assuming instead that $\sup_{x \in \mathcal{X}} p^*(x)/\bar{p}(x) = M_{p^*, \bar{p}} < \infty$, then*

$$\text{var}_{\bar{p}}(p^*/\bar{p}) \leq C_m D_H(p^*, \bar{p})^2, \quad \text{where } C_m = 4 + 4M_{p^*, \bar{p}}.$$

Proof. Proof of the first result. Because $\tilde{g}^{(\ell)}(x)^2 \geq 0$ and $\lambda(x) \geq 0$ for all $x \in \mathcal{X}$, the density $\bar{p}(x)$ satisfies

$$\bar{p}(x) \geq \lambda(x) \left\{ \prod_{\ell=1}^L \frac{\tau^{(\ell)}}{\zeta^{(\ell)}} \right\} \quad (\text{D.1})$$

for all $x \in \mathcal{X}$, which leads to $\text{supp}(\lambda) \subseteq \text{supp}(\bar{p})$. Under Assumption 3, we have $\text{supp}(\rho^*) \subseteq \text{supp}(\lambda) \subseteq \text{supp}(\bar{p})$, and thus we can express ζ^* as

$$\zeta^* = \int_{\mathcal{X}} \frac{\rho^*(x)}{\pi_0(x)} \pi_0(x) dx = \int_{\mathcal{X}} \frac{\rho^*(x)}{\bar{p}(x)} \bar{p}(x) dx.$$

Furthermore, the identity in (D.1) also leads to

$$\frac{\pi_0(x)}{\bar{p}(x)} \leq \frac{\pi_0(x)}{\lambda(x)} \left\{ \prod_{\ell=1}^L \frac{\zeta^{(\ell)}}{\tau^{(\ell)}} \right\}.$$

Together with Assumption 3, we also have $\sup_{x \in \mathcal{X}} \pi_0(x)/\bar{p}(x) < \infty$. This way, the second moment $E_{\bar{p}}[(\rho^*/\bar{p})^2]$ satisfies

$$E_{\bar{p}} \left\{ \left(\frac{\rho^*}{\bar{p}} \right)^2 \right\} = \int_{\mathcal{X}} \left\{ \frac{\rho^*(x)}{\pi_0(x)} \right\}^2 \frac{\pi_0(x)}{\bar{p}(x)} \pi_0(x) dx \leq E_{\pi_0} \left\{ \left(\frac{\rho^*}{\pi_0} \right)^2 \right\} \sup_{x \in \mathcal{X}} \frac{\pi_0(x)}{\bar{p}(x)}.$$

Then, applying Assumption 2, we have $E_{\bar{p}}\{(\rho^*/\bar{p})^2\} < \infty$. Thus, the result follows.

Proof of the second and third results. Recall that the relative variance takes the form $\text{var}_{\bar{p}}(p^*/\bar{p}) = E_{\bar{p}}\{(p^*/\bar{p})^2\} - E_{\bar{p}}\{p^*/\bar{p}\}^2$, where $E_{\bar{p}}\{p^*/\bar{p}\} = 1$. Together with $\text{supp}(p^*) \subseteq \text{supp}(\bar{p})$ in the first result, the relative variance can be expressed as

$$\begin{aligned} \text{var}_{\bar{p}}(p^*/\bar{p}) &= E_{\bar{p}}\{(p^*/\bar{p})^2\} - 1 \\ &= E_{p^*}(p^*/\bar{p}) - E_{\bar{p}}(p^*/\bar{p}) \\ &= \int_{\mathcal{X}} \frac{p^*(x)}{\bar{p}(x)} \bar{p}(x) dx - \int_{\mathcal{X}} \frac{p^*(x)}{\bar{p}(x)} \bar{p}(x) dx - \int_{\mathcal{X}} p^*(x) dx + \int_{\mathcal{X}} \bar{p}(x) dx \\ &= \int_{\mathcal{X}} \left\{ \frac{p^*(x)}{\bar{p}(x)} - 1 \right\} p^*(x) dx - \int_{\mathcal{X}} \left\{ \frac{p^*(x)}{\bar{p}(x)} - 1 \right\} \bar{p}(x) dx \\ &= \int_{\mathcal{X}} \left\{ \frac{p^*(x)}{\bar{p}(x)} - 1 \right\} \{p^*(x) - \bar{p}(x)\} dx \\ &= \int_{\mathcal{X}} \left\{ \frac{p^*(x)}{\bar{p}(x)} - 1 \right\} \{\sqrt{p^*(x)} + \sqrt{\bar{p}(x)}\} \{\sqrt{p^*(x)} - \sqrt{\bar{p}(x)}\} dx. \end{aligned} \quad (\text{D.2})$$

Apply the Cauchy-Schwartz inequality to (D.2), the relative variance has the bound

$$\begin{aligned} \text{var}_{\bar{p}}(p^*/\bar{p}) &\leq \left[\int_{\mathcal{X}} \left\{ \frac{p^*(x)}{\bar{p}(x)} - 1 \right\}^2 \{\sqrt{p^*(x)} + \sqrt{\bar{p}(x)}\}^2 dx \right]^{\frac{1}{2}} \left[\int_{\mathcal{X}} \{\sqrt{p^*(x)} - \sqrt{\bar{p}(x)}\}^2 dx \right]^{\frac{1}{2}} \\ &= \left[\int_{\mathcal{X}} \left\{ \frac{p^*(x)}{\bar{p}(x)} - 1 \right\}^2 \{\sqrt{p^*(x)} + \sqrt{\bar{p}(x)}\}^2 dx \right]^{\frac{1}{2}} \sqrt{2} D_{\text{H}}(p^*, \bar{p}). \end{aligned} \quad (\text{D.3})$$

Depending on the assumption imposed on the ratio p^*/\bar{p} , the upper bound of $\text{var}_{\bar{p}}(p^*/\bar{p})$ depends differently on the Hellinger error. We note that

$$\begin{aligned} &\left[\int_{\mathcal{X}} \left\{ \frac{p^*(x)}{\bar{p}(x)} - 1 \right\}^2 \{\sqrt{p^*(x)} + \sqrt{\bar{p}(x)}\}^2 dx \right]^{\frac{1}{2}} \\ &\leq \left[\int_{\mathcal{X}} \left\{ \frac{p^*(x)}{\bar{p}(x)} - 1 \right\}^2 p^*(x) dx \right]^{\frac{1}{2}} + \left[\int_{\mathcal{X}} \left\{ \frac{p^*(x)}{\bar{p}(x)} - 1 \right\}^2 \bar{p}(x) dx \right]^{\frac{1}{2}} \\ &\leq \sqrt{2} \left[\int_{\mathcal{X}} \left\{ \frac{p^*(x)}{\bar{p}(x)} - 1 \right\}^2 p^*(x) dx + \int_{\mathcal{X}} \left\{ \frac{p^*(x)}{\bar{p}(x)} - 1 \right\}^2 \bar{p}(x) dx \right]^{\frac{1}{2}} \\ &= \sqrt{2} \left[\int_{\mathcal{X}} \left\{ \frac{p^*(x)}{\bar{p}(x)} \right\}^2 p^*(x) dx - \int_{\mathcal{X}} \left\{ \frac{p^*(x)}{\bar{p}(x)} \right\}^2 \bar{p}(x) dx \right]^{\frac{1}{2}} \\ &= \sqrt{2} [E_{p^*}\{(p^*/\bar{p})^2\} - E_{\bar{p}}\{(p^*/\bar{p})^2\}]^{\frac{1}{2}}. \end{aligned} \quad (\text{D.4})$$

Note that $E_{p^*}\{(p^*/\bar{p})^2\} \geq \{E_{p^*}(p^*/\bar{p})\}^2$ and $E_{\bar{p}}\{(p^*/\bar{p})^2\} \geq \{E_{\bar{p}}(p^*/\bar{p})\}^2 = 1$ by Jensen's inequality. Together with $E_{p^*}(p^*/\bar{p}) = E_{\bar{p}}\{(p^*/\bar{p})^2\}$, the difference on the right hand side of (D.4) is non-negative. That is,

$$E_{p^*}\{(p^*/\bar{p})^2\} - E_{\bar{p}}\{(p^*/\bar{p})^2\} \geq 0.$$

In addition, we have

$$E_{p^*}\{(p^*/\bar{p})^2\} = E_{\bar{p}}\{(p^*/\bar{p})^3\} = \frac{1}{(\zeta^*)^3} E_{\bar{p}}\{(\rho^*/\bar{p})^3\} < \infty,$$

which can be obtained using a similar derivation as in the proof of the first result and the assumption that the ratio ρ^*/π_0 has finite third moment with respect to π_0 . Thus, we have the upper bound

$$\text{var}_{\bar{p}}(p^*/\bar{p}) \leq 2 [E_{p^*}\{(p^*/\bar{p})^2\} - E_{\bar{p}}\{(p^*/\bar{p})^2\}]^{\frac{1}{2}} D_{\text{H}}(p^*, \bar{p}),$$

which concludes the second result of this Lemma.

With a more restrictive assumption $\sup_{x \in \mathcal{X}} p^*(x)/\bar{p}(x) = M_{p^*, \bar{p}} < \infty$, we can also use the identity

$$\begin{aligned} \left[\int_{\mathcal{X}} \left\{ \frac{p^*(x)}{\bar{p}(x)} - 1 \right\}^2 \{ \sqrt{p^*(x)} + \sqrt{\bar{p}(x)} \}^2 dx \right]^{\frac{1}{2}} &= \left[\int_{\mathcal{X}} \left\{ \frac{\sqrt{p^*(x)}}{\sqrt{\bar{p}(x)}} + 1 \right\}^4 \{ \sqrt{p^*(x)} - \sqrt{\bar{p}(x)} \}^2 dx \right]^{\frac{1}{2}} \\ &\leq \left[\sup_{x \in \mathcal{X}} \left\{ \frac{\sqrt{p^*(x)}}{\sqrt{\bar{p}(x)}} + 1 \right\}^4 2 D_{\text{H}}(p^*, \bar{p})^2 \right]^{\frac{1}{2}} \\ &= \sqrt{2} (1 + \sqrt{M_{p^*, \bar{p}}})^2 D_{\text{H}}(p^*, \bar{p}) \\ &\leq 2\sqrt{2} (1 + \sqrt{M_{p^*, \bar{p}}}) D_{\text{H}}(p^*, \bar{p}) \end{aligned} \quad (\text{D.5})$$

Plugging the above identity into (D.3), we obtain the upper bound

$$\text{var}_{\bar{p}}(p^*/\bar{p}) \leq (4 + 4M_{p^*, \bar{p}}) D_{\text{H}}(p^*, \bar{p})^2.$$

This concludes the third result of this Lemma. \square

APPENDIX E. PROOF OF LEMMAS 3 AND 4

Appendix E.1. Taylor series of the relative deviation $\Delta_{R,N}$

The following results are useful for showing Lemmas 3 and 4. To analyze the asymptotic properties of $\Delta_{R,N} = \hat{Q}_{\bar{p},N}/\hat{Z}_{\bar{q},N}$, we introduce the relative derivations of $\hat{Q}_{\bar{p},N}$ and $\hat{Z}_{\bar{q},N}$, which are given by

$$\Delta_{Q,N} = (\hat{Q}_{\bar{p},N} - Q)/Q, \quad \Delta_{Z,N} = (\hat{Z}_{\bar{q},N} - Z)/Z,$$

respectively. Using random variables $W_Q = w_Q(U_p)$ and $W_Z = w_Z(U_q)$, we can define

$$\Theta_Q := \frac{W_Q}{Q} - 1, \quad \Theta_Z := \frac{W_Z}{Z} - 1,$$

such that

$$\Delta_{Q,N} = \frac{1}{N} \sum_{i=1}^N \Theta_Q^i, \quad \Delta_{Z,N} = \frac{1}{N} \sum_{i=1}^N \Theta_Z^i. \quad (\text{E.1})$$

Note that we have $E(\Theta_Q) = 0$ and $E(\Theta_Z) = 0$ by construction as $E(W_Q) = Q$ and $E(W_Z) = Z$. Thus, $\Delta_{Q,N}$ and $\Delta_{Z,N}$ have zero expected values for any sample size N . Furthermore, using $\text{var}(W_Q)$, $\text{var}(W_Z)$ and $\text{cov}(W_Q, W_Z)$, the variances and the covariance of Θ_Q and Θ_Z can be given as

$$\text{var}(\Theta_Q) = \frac{\text{var}(W_Q)}{Q^2}, \quad \text{var}(\Theta_Z) = \frac{\text{var}(W_Z)}{Z^2}, \quad \text{cov}(\Theta_Q, \Theta_Z) = \frac{\text{cov}(W_Q, W_Z)}{QZ}. \quad (\text{E.2})$$

The relative deviation of $\hat{R}_{\bar{p},\bar{q},N}$ from the *a posteriori* expectation R can be expressed as

$$\Delta_{R,N} = \frac{\hat{R}_{\bar{p},\bar{q},N} - R}{R} = \frac{Z}{Q} \left(\frac{\hat{Q}_{\bar{p},N}}{\hat{Z}_{\bar{q},N}} - \frac{Q}{Z} \right) = \frac{1 + \Delta_{Q,N}}{1 + \Delta_{Z,N}} - 1 = \frac{\Delta_{Q,N} - \Delta_{Z,N}}{1 + \Delta_{Z,N}}.$$

Applying Taylor's theorem, there exist some $s, t \in [0, 1]$ such that

$$\frac{1}{1 + \Delta_{Z,N}} = 1 - \frac{1}{(1 + s\Delta_{Z,N})^2} \Delta_{Z,N}, \quad (\text{E.3})$$

$$\frac{1}{1 + \Delta_{Z,N}} = 1 - \Delta_{Z,N} + \frac{1}{(1 + t\Delta_{Z,N})^3} \Delta_{Z,N}^2, \quad (\text{E.4})$$

where s and t depend on $\Delta_{Z,N}$. Note that the term $1 + s\Delta_{Z,N}$ (and similarly $1 + t\Delta_{Z,N}$) satisfies

$$1 + s\Delta_{Z,N} = (1 - s) + s(1 + \Delta_{Z,N}) = (1 - s) + s \frac{\hat{Z}_{\bar{q},N}}{Z} > 0$$

almost surely, because the estimator $\hat{Z}_{\bar{q},N}$ is almost surely positive by construction. Thus, the expansions in (E.3) and (E.4) are not subject to division-by-zero.

Appendix E.2. Asymptotic distribution of $\sqrt{N}\Delta_{R,N}$

LEMMA 3. *Suppose Assumptions 1–3 hold and the sequence $\{(W_Q^i, W_Z^i)\}_{i=1}^N$ is independent and identically distributed, but allowing each pair (W_Q^i, W_Z^i) to be correlated. Then, $\sqrt{N}\Delta_{R,N}$ converges in distribution to*

$$\mathcal{N} \left\{ 0, \frac{\text{var}(W_Q)}{Q^2} + \frac{\text{var}(W_Z)}{Z^2} - \frac{2\text{cov}(W_Q, W_Z)}{QZ} \right\}.$$

Proof. Using the expansion (E.3), we have

$$\sqrt{N}\Delta_{R,N} = \sqrt{N}(\Delta_{Q,N} - \Delta_{Z,N}) - \frac{\Delta_{Z,N}}{(1 + s\Delta_{Z,N})^2} \sqrt{N}(\Delta_{Q,N} - \Delta_{Z,N}).$$

Recall the sample average definition of $\Delta_{Q,N}$ and $\Delta_{Z,N}$ in (E.1), we have

$$\Delta_{Q,N} - \Delta_{Z,N} = \frac{1}{N} \sum_{i=1}^N (\Theta_Q^i - \Theta_Z^i),$$

and hence $\sqrt{N}(\Delta_{Q,N} - \Delta_{Z,N})$ converges in distribution to $\mathcal{N}\{0, \text{var}(\Theta_Q - \Theta_Z)\}$ by the central limit theorem, where $\text{var}(\Theta_Q - \Theta_Z) = \text{var}(\Theta_Q) + \text{var}(\Theta_Z) - 2\text{cov}(\Theta_Q, \Theta_Z)$. Since the sequence $\Delta_{Z,N}$ converge to zero in probability as N tends to infinity, i.e., $\Delta_{Z,N} = o_p(1)$ and the sequence $\sqrt{N}(\Delta_{Q,N} - \Delta_{Z,N})$ is tight, applying Slutsky's theorem and the identities in (E.2), we have $\sqrt{N}\Delta_{R,N}$ converges in distribution to

$$\mathcal{N} \left\{ 0, \frac{\text{var}(W_Q)}{Q^2} + \frac{\text{var}(W_Z)}{Z^2} - \frac{2\text{cov}(W_Q, W_Z)}{QZ} \right\}.$$

This gives the Asymptotic distribution of $\sqrt{N}\Delta_{R,N}$. \square

Appendix E.3. Bias of $\hat{R}_{\bar{p},\bar{q},N}$

LEMMA 4. *Under the assumptions of Lemma 3, but now assuming furthermore independence of the sequences $\{W_Q^i\}_{i=1}^N$ and $\{W_Z^i\}_{i=1}^N$ as well, the relative bias of $\hat{R}_{\bar{p},\bar{q},N}$ as $N \rightarrow \infty$ satisfies*

$$\frac{N|E(\hat{R}_{\bar{p},\bar{q},N}) - R|}{R} \rightarrow \frac{\text{var}(W_Z)}{Z^2},$$

and the relative mean square error of $\hat{R}_{\bar{p}, \bar{q}, N}$ satisfies

$$\text{rmse}(\hat{R}_{\bar{p}, \bar{q}, N}, R) = \mathcal{O} \left\{ \frac{C_p D_H(p^*, \bar{p}) + C_q D_H(q^*, \bar{q})}{N} + \frac{1}{N^2} \right\}, \quad (23)$$

where $C_p = 2[E_{p^*}\{(p^*/\bar{p})^2\} - E_{\bar{p}}\{(p^*/\bar{p})^2\}]^{1/2}$ and $C_q = 2[E_{q^*}\{(q^*/\bar{q})^2\} - E_{\bar{q}}\{(q^*/\bar{q})^2\}]^{1/2}$.

Proof. Using (E.4), the expected relative deviation $\Delta_{R,N}$ can be expressed as

$$E(\Delta_{R,N}) = E(\Delta_{Q,N} - \Delta_{Z,N}) - E\{(\Delta_{Q,N} - \Delta_{Z,N})\Delta_{Z,N}\} + E \left\{ \Delta_{Z,N}^2 \frac{\Delta_{Q,N} - \Delta_{Z,N}}{(1 + t\Delta_{Z,N})^3} \right\},$$

where $t \in [0, 1]$ depending on $\Delta_{Z,N}$. Recall the sample average definition of $\Delta_{Q,N}$ and $\Delta_{Z,N}$ in (E.1). Since we have $E(\Theta_Q) = 0$ and $E(\Theta_Z) = 0$, the relative deviations $\Delta_{Q,N}$ and $\Delta_{Z,N}$ satisfy $E(\Delta_{Q,N}) = 0$ and $E(\Delta_{Z,N}) = 0$ for any given sample size N . With the additional assumption that the sequences $\{W_Q^i\}_{i=1}^N$ and $\{W_Z^i\}_{i=1}^N$ are independent, we have that $\{\Theta_Q^i\}_{i=1}^N$ and $\{\Theta_Z^i\}_{i=1}^N$ are also independent. Therefore, we have mutually independent $\Delta_{Q,N}$ and $\Delta_{Z,N}$ for all N . Thus, the expected relative deviation can be simplified as

$$\begin{aligned} E(\Delta_{R,N}) &= E(\Delta_{Q,N}) - E(\Delta_{Z,N}) - E(\Delta_{Q,N})E(\Delta_{Z,N}) + E \left[\Delta_{Z,N}^2 \left\{ 1 + \frac{\Delta_{Q,N} - \Delta_{Z,N}}{(1 + t\Delta_{Z,N})^3} \right\} \right] \\ &= E \left[\Delta_{Z,N}^2 \left\{ 1 + \frac{\Delta_{Q,N} - \Delta_{Z,N}}{(1 + t\Delta_{Z,N})^3} \right\} \right]. \end{aligned}$$

Thus, we can introduce a random variable

$$B_N = \Delta_{Z,N}^2 \left\{ 1 + \frac{\Delta_{Q,N} - \Delta_{Z,N}}{(1 + t\Delta_{Z,N})^3} \right\}$$

such that the relative bias of $\hat{R}_{\bar{p}, \bar{q}, N}$ satisfies

$$\frac{|E(\hat{R}_{\bar{p}, \bar{q}, N}) - R|}{R} = |E(\Delta_{R,N})| = |E(B_N)|.$$

We want to use Slutsky's theorem to examine the property of the sequence

$$\frac{NB_N}{\text{var}(\Theta_Z)} = \left\{ \frac{\sqrt{N}\Delta_{Z,N}}{\sqrt{\text{var}(\Theta_Z)}} \right\}^2 \left\{ 1 + \frac{\Delta_{Q,N} - \Delta_{Z,N}}{(1 + t\Delta_{Z,N})^3} \right\}.$$

Since $\sqrt{N}\Delta_{Z,N}$ converges in distribution to $\mathcal{N}\{0, \text{var}(\Theta_Z)\}$, we have the ratio $\sqrt{N}\Delta_{Z,N}/\sqrt{\text{var}(\Theta_Z)}$ converges in distribution to $\mathcal{N}(0, 1)$. Then, the continuous mapping theorem implies that the term $\{\sqrt{N}\Delta_{Z,N}/\sqrt{\text{var}(\Theta_Z)}\}^2$ converges in distribution to the random variable ξ^2 , where $\xi \sim \mathcal{N}(0, 1)$.

Note that ξ^2 follows the chi-squared distribution with one degree of freedom, i.e., $\xi^2 \sim \chi_1^2$, and hence we equivalently have $\{\sqrt{N}\Delta_{Z,N}/\sqrt{\text{var}(\Theta_Z)}\}^2$ converges in distribution to χ_1^2 . Since $\Delta_{Z,N} = o_p(1)$ and $\Delta_{Q,N} = o_p(1)$, we have $NB_N/\text{var}(\Theta_Z)$ converges in distribution to χ_1^2 by Slutsky's theorem. Thus, by the Portmanteau lemma, we have $E\{NB_N/\text{var}(\Theta_Z)\} \rightarrow 1$ as $N \rightarrow \infty$. Therefore, applying the identities in (E.2), as $N \rightarrow \infty$ the asymptotic behaviour of the relative bias satisfies

$$\frac{N|E(\hat{R}_{\bar{p}, \bar{q}, N}) - R|}{R} \rightarrow \frac{\text{var}(W_Z)}{Z^2}.$$

Thus, the relative bias is asymptotically $\mathcal{O}(N^{-1})$.

With the additional assumption that the sequences $\{W_Q^i\}_{i=1}^N$ and $\{W_Z^i\}_{i=1}^N$ are also independent, we have $\text{cov}(W_Q, W_Z) = 0$. Applying the result of Lemma 3, the relative mean square error of $\hat{R}_{\bar{p}, \bar{q}, N}$ asymptotically follows

$$\text{rmse}(\hat{R}_{\bar{p}, \bar{q}, N}, R) = \mathcal{O} \left\{ \frac{\text{var}(W_Q)}{NQ^2} + \frac{\text{var}(W_Z)}{NZ^2} + \frac{1}{N^2} \right\}.$$

Since $\text{var}(W_Q)/Q^2 = \text{var}_{\bar{p}}(p^*/\bar{p})$ and $\text{var}(W_Z)/Z^2 = \text{var}_{\bar{q}}(q^*/\bar{q})$, the rest of the proof directly follows from the second result of Lemma 2. \square

APPENDIX F. SMOOTHING ERROR IN RARE EVENT ESTIMATION

As suggested by Lemma 2, the efficiency of the resulting importance sampling estimator is controlled by the Hellinger error between the original optimal importance density and its approximation, i.e., $D_H(p^*, \bar{p})$. We can split the Hellinger error using the triangle inequality,

$$D_H(p^*, \bar{p}) \leq D_H(p^*, p_{\gamma^*}) + D_H(p_{\gamma^*}, \bar{p}),$$

where the first term on the right-hand-side represents the error due to smoothing while the second term represents the error in the construction of the deep inverse Rosenblatt transport. As discussed already previously, if one aims for a small smoothing error by choosing a rather large γ^* , then the smoothed optimal importance density can be computationally costly to approximate. It may need many layers of bridging densities and the required tensor-train decompositions will in general have high ranks. On the other hand, smaller values of γ^* make it computationally easier to reduce the tensor-train approximation error, but then the total Hellinger error will be dominated by the smoothing error.

In practice, we want to balance the two error sources $D_H(p^*, p_{\gamma^*})$ and $D_H(p_{\gamma^*}, \bar{p})$. We derive the following heuristic to understand the impact of the smoothing variable γ on the Hellinger error $D_H(p^*, p_\gamma)$. We conjecture that, if the system response function h and the prior density π_0 are Lipschitz, then the smoothing error $D_H(p^*, p_\gamma)$ is about $\mathcal{O}(\gamma^{-1/2})$. Under more relaxed assumptions, the smoothing error $D_H(p^*, p_\gamma)$ may be about $\mathcal{O}(\gamma^{-1/4})$.

To obtain some insights into those claims, we consider the output of the response function, $H = h(X)$, $X \sim \pi_0$, which is a random variable with the law

$$\text{pr}(H < z) = \int \mathbf{1}_{[z, \infty)}\{h(x)\}\pi_0(x)dx,$$

such that H has the probability density

$$\varphi(z) = \int \delta(z - h(x))\pi_0(x)dx.$$

We recall the optimal importance density and its smoothed version

$$p^*(x) \propto \rho^*(x) := \mathbf{1}_{[a, \infty)}(h(x))\pi_0(x), \quad (\text{F.1})$$

$$p_\gamma(x) \propto \rho_\gamma(x) := f_\gamma(z; [a, \infty))\pi_0(x). \quad (\text{F.2})$$

Following a similar derivation as in Appendix A, we have

$$D_H(p^*, p_\gamma) \leq \frac{\sqrt{2}}{\sqrt{\zeta^*}} \|\sqrt{\rho^*} - \sqrt{\rho_\gamma}\|, \quad (\text{F.3})$$

where $\zeta^* = \int_{\mathcal{X}} \rho^*(x)dx$. Note that the above expression does not have an extra factor of $\sqrt{2}$, as in Appendix A, because the tensor-train approximation in Appendix A contains the regularising term involving τ times the reference density. The squared error $\mathcal{E}(\gamma)^2 := \|\sqrt{\rho^*} - \sqrt{\rho_\gamma}\|^2$ can be expressed as

$$\begin{aligned} \mathcal{E}(\gamma)^2 &= \int \left(\mathbf{1}_{[a, \infty)}\{h(x)\}^{1/2} - f_\gamma\{h(x); [a, \infty)\}^{1/2} \right)^2 \pi_0(x)dx \\ &= \int \left[\mathbf{1}_{[a, \infty)}(z) - f_\gamma\{z; [a, \infty)\}^{1/2} \right]^2 \delta(z - h(x))\pi_0(x)dz dx \\ &= \int \left[\mathbf{1}_{[a, \infty)}(z) - f_\gamma\{z; [a, \infty)\}^{1/2} \right]^2 \varphi(z)dz, \end{aligned} \quad (\text{F.4})$$

which is the function $[\mathbf{1}_{[a, \infty)}(z) - f_\gamma\{z; [a, \infty)\}^{1/2}]^2$ weighted by the density $\varphi(z)$. Figure 6 shows an example of $[\mathbf{1}_{[a, \infty)}(z) - f_\gamma\{z; [a, \infty)\}^{1/2}]^2$ for various values of γ , where f_γ is the sigmoid function in

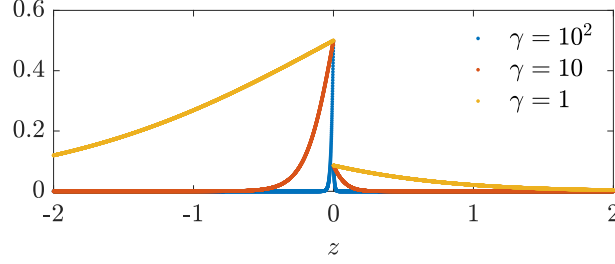


Fig. 6: The function $(1_{[0, \infty)}(z) - \sqrt{f_\gamma(z; [0, \infty))})^2$ with different values of γ .

(24). Since the function $[1_{[a, \infty)}(z) - f_\gamma\{z; [a, \infty)\}]^{1/2}$ has shrinking area under the curve with increasing γ , the squared error $\mathcal{E}(\gamma)^2$ depends on the rate this area shrinks with respect to the density function $\varphi(z)$.

Considering the sigmoid function (24) as the smoothing surrogate, we have

$$\left[1_{[a, \infty)}(z) - f_\gamma\{z; [a, \infty)\}\right]^{1/2} \leq \frac{1}{1 + \exp(\gamma|z - a|)},$$

and thus, by Hölder's inequality, $\mathcal{E}(\gamma)^2$ satisfies

$$\mathcal{E}(\gamma)^2 \leq \int \frac{1}{1 + \exp(\gamma|z - a|)} \varphi(z) dz \leq \left[\int \frac{1}{\{1 + \exp(\gamma|z - a|)\}^s} dz \right]^{1/s} \left\{ \int \varphi(z)^t dz \right\}^{1/t},$$

for any $s, t \geq 1$ with $s^{-1} + t^{-1} = 1$. Under the minimal assumption that $\int \varphi(z) dz = 1$, since $\varphi(z)$ is a probability density function, we can only choose $s = \infty$ and $t = 1$, such that

$$\mathcal{E}(\gamma)^2 \leq \sup_z \frac{1}{1 + \exp(\gamma|z - a|)} = \frac{1}{2}$$

and the squared error does not reduce for $\gamma \rightarrow \infty$. Under the more restrictive assumption that $\int \varphi(z)^2 dz < \infty$ we can have $s = t = 2$, and hence

$$\mathcal{E}(\gamma)^2 \leq \int \frac{1}{1 + \exp(\gamma|z - a|)} \varphi(z) dz \leq \left[\int \frac{1}{\{1 + \exp(\gamma|z - a|)\}^2} dz \right]^{1/2} \left\{ \int \varphi(z)^2 dz \right\}^{1/2},$$

Using the change of variable $\alpha = \gamma(z - a)$, this leads to

$$\int \frac{1}{\{1 + \exp(\gamma|z - a|)\}^2} dz = \frac{1}{\gamma} \int \frac{1}{\{1 + \exp(|\alpha|)\}^2} d\alpha = \frac{2 \log 2 - 1}{\gamma},$$

and thus

$$D_H(p^*, p_\gamma) \leq \frac{\sqrt{2}}{\sqrt{\zeta^*}} \left\{ \int \varphi(z)^2 dz \right\}^{1/4} (2 \log 2 - 1)^{1/4} \gamma^{-1/4}.$$

Alternatively, if we assume that density $\varphi(z)$ is bounded, we can set $s = 1$ and $t = \infty$, which gives

$$\mathcal{E}(\gamma)^2 \leq \int \frac{1}{1 + \exp(\gamma|z - a|)} \varphi(z) dz \leq \left\{ \int \frac{1}{1 + \exp(\gamma|z - a|)} dz \right\} \sup_z \varphi(z),$$

and thus the same change of variable $\alpha = \gamma(z - a)$ leads to

$$D_H(p^*, p_\gamma) \leq 2 \left\{ \frac{\log 2 \sup_z \varphi(z)}{\zeta^*} \right\}^{1/2} \gamma^{-1/2}.$$

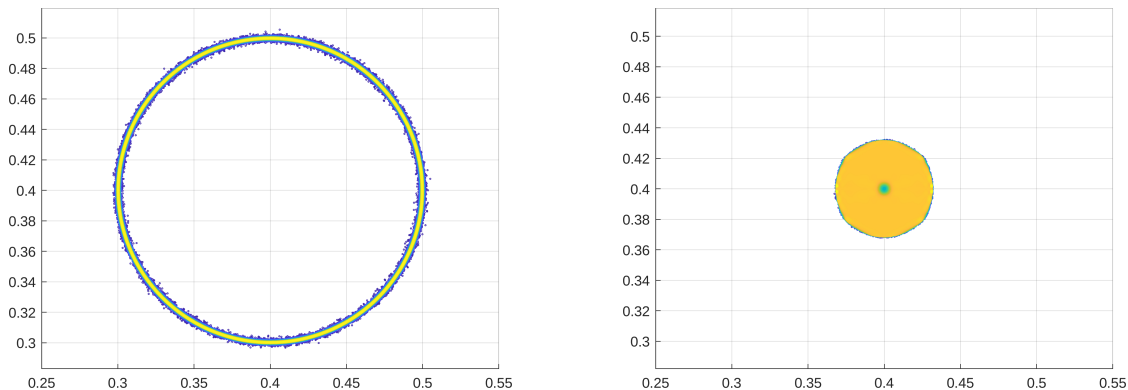


Fig. 7: Samples drawn from the approximate importance densities, colored by their density values, for $R_o^2 = 10^{-2}$, $R_i^2 = R_o^2 - 10^{-4}$ (left) and for $R_o^2 = 10^{-3}$, $R_i^2 = 0$ (right).

We conjecture that having both Lipschitz $h(x)$ and $\pi_0(x)$ may be sufficient to provide an upper bound to the density $\varphi(z)$, but we have no proof for this claim. In this derivation, the dependency of the squared error on γ is essentially obtained via the change of variable $\alpha = \gamma(z - a)$. Thus, for other smoothing functions, e.g., the distribution function of a Gaussian random variable with γ as the inverse of the variance, we expect similar results to hold.

APPENDIX G. AREAS OF ANNULUS AND DISK

We consider a 2-dimensional toy example for estimating *a priori* failure probabilities, where the prior distribution that is uniform on the unit square, i.e., $\pi_0(x) = 1$ with $x \in [0, 1]^2$ and the failure function

$$f(x) = \mathbf{1}_{\{R_i \leq \|x - x_0\|_2 \leq R_o\}}(x), \quad (\text{G.1})$$

for given radii $0 \leq R_i < R_o$ and center $x_0 = [0.4, 0.4]$. Thus, the event probability is the area of the annulus, $\zeta^* := \text{pr}_{\pi_0}(X \in \mathcal{A}) = \text{Pi}(R_o^2 - R_i^2)$, where Pi is Archimedes' constant.

The smoothed indicator function for Alg. 1 is defined as a product of two sigmoids,

$$f_\gamma(x) = [1 + \exp\{\gamma(\|x - x_0\|_2^2 - R_o^2)\}]^{-1} [1 + \exp\{\gamma(R_i^2 - \|x - x_0\|_2^2)\}]^{-1}.$$

To approximate the smoothed optimal importance density with Alg. 1, we tune various control variables in the deep importance sampling procedure such that the Hellinger distance between the approximate density and the optimal importance density $p^*(x)$ is about 0.3 for all choices of R_i and R_o . This involves varying the final smoothing variable $\gamma_L = \gamma^*$, the univariate grid size n , the tensor rank r , and the initial smoothing variable γ_1 . The intermediate bridging densities are defined throughout by $\gamma_{\ell+1} = \sqrt{10} \gamma_\ell$. Once the approximation of the optimal importance density is computed, we use $N = 2^{16}$ samples to compute the deep importance sampling estimator $\hat{\zeta}_{\bar{p}, N}$ in (20).

In the first experiment, we fix the outer radius $R_o = 0.1$, and vary the inner radius R_i , as shown in Fig. 7 (left), such that it approaches R_o . The results are shown in Table 2. This setup requires finer discretizations, that is, larger values of n , as the width of the annulus decreases. As a result, the number of function evaluations to approximate the optimal importance density, N_{TT} , grows rapidly.

In contrast, if the inner radius is fixed to $R_i = 0$ and the outer radius R_o is varied, the optimal importance density function $p^*(x) \propto f(x)\pi_0(x)$ is unimodal, representing just the indicator function of the disk with radius R_o . As we can see in Table 3, in that case the approximation complexity, in terms of function evaluations, depends only logarithmically on the value of ζ^* .

Table 2: Annulus test with $R_o = 0.1$ fixed. N_{TT} is the total number of function evaluations used in Alg. 1 to approximate the smoothed optimal importance density. The last column gives the relative bias of the estimator in each case.

$R_o^2 - R_i^2$	γ^*	n	r	γ_1	N_{TT}	$D_H(p^*, \bar{p})$	$ \hat{\zeta}_{\bar{p}, N} - \zeta^* /\zeta^*$
10^{-3}	10^4	33	3	10^{-3}	1386	0.308 ± 0.0014	0.00244 ± 0.00114
10^{-4}	10^5	65	3	10^{-4}	3510	0.292 ± 0.0033	0.00162 ± 0.00158
10^{-5}	10^6	257	5	10^{-4}	23130	0.292 ± 0.0159	0.00293 ± 0.00570
10^{-6}	10^7	513	10	10^{-5}	112860	0.304 ± 0.0111	0.00232 ± 0.00180
10^{-7}	10^8	1025	20	10^{-6}	533000	0.379 ± 0.0320	0.00616 ± 0.00445

Table 3: Disk test with $R_i = 0$ fixed. N_{TT} is the total number of function evaluations used in Alg. 1 for approximating the smoothed optimal importance densities. The last column gives the relative bias of the estimator in each case.

R_o^2	γ^*	n	r	γ_1	N_{TT}	$D_H(p^*, \bar{p})$	$ \hat{\zeta}_{\bar{p}, N} - \zeta^* /\zeta^*$
10^{-2}	10^3	17	2	10^{-2}	340	0.224 ± 0.0015	0.00136 ± 0.00094
10^{-3}	10^4	17	2	10^{-2}	340	0.221 ± 0.0036	0.00111 ± 0.00078
10^{-4}	10^5	17	2	10^{-3}	476	0.218 ± 0.0017	0.00105 ± 0.00090
10^{-5}	10^6	17	2	10^{-4}	612	0.218 ± 0.0015	0.00144 ± 0.00095
10^{-6}	10^7	17	2	10^{-5}	748	0.218 ± 0.0015	0.00193 ± 0.00100
10^{-7}	10^8	17	2	10^{-5}	748	0.222 ± 0.0041	0.00105 ± 0.00072

APPENDIX H. BAYESIAN INFERENCE OF THE ELLIPTIC PDE

Appendix H.1. Model discretization

Considering spatial coordinates $s, t \in D$, the logarithm of the diffusivity field is assumed to be a zero mean Gaussian process with the Matérn covariance function

$$C(s, t) = \frac{2^{1-\nu}}{\Gamma(\nu)} \left(\sqrt{2\nu} \frac{\|s - t\|_2}{\ell} \right)^\nu K_\nu \left(\sqrt{2\nu} \frac{\|s - t\|_2}{\ell} \right),$$

where ν is the smoothness parameter, and ℓ is the correlation length. This definition includes the Gaussian covariance function as the limit $\nu \rightarrow \infty$. Applying the Karhunen-Lóve expansion, the infinite-dimensional field $\log \kappa(s, X)$ yields a truncated representation

$$\log \kappa(s, X) = \sum_{k=1}^d X_k \sqrt{\lambda_k} \psi_k(s), \quad (\text{H.1})$$

where $\{\psi_k(s), \lambda_k\}$ is the k th eigenpair of the covariance operator associated with $C(s, t)$, that is

$$\int_D C(s, t) \psi_k(t) dt = \lambda_k \psi_k(s).$$

In the series expansion, the random field $\log \kappa(s, X)$ is equivalently characterised by the coefficients X_1, X_2, \dots , where each coefficient follows a standard Gaussian distribution. Thus, the prior distribution over $X = (X_1, \dots, X_d)$ after truncation takes the form

$$\pi_0(x) \propto \prod_{k=1}^d \exp \left(-\frac{1}{2} x_k^2 \right). \quad (\text{H.2})$$

For each realization of X , we first apply the Galerkin method with continuous, bilinear finite elements to numerically solve the partial differential equation

$$-\nabla \cdot \{\kappa(s, X) \nabla u(s, X)\} = 0, \quad s \in (0, 1)^2, \quad (\text{H.3})$$

with boundary conditions as specified in each numerical test. The finite element solution u_h is computed on a uniform rectangular grid on D with a mesh size $h = 1/64$ along each of the coordinates of the physical domain. Then, the inhomogeneous horizontal Darcy flow field $\kappa(s, X) \nabla u_h(s, X)$ is also calculated in the same finite element space.

Finally, we numerically solve the ordinary differential equation

$$\frac{ds(t, X)}{dt} = \kappa(s, X) \nabla u_h(s, X), \quad s(0, X) = s^0, \quad (\text{H.4})$$

to approximate the breakthrough time $\tau(X)$ for a particle to traverse from $s_0 = (0, 0.5)$ to the right boundary of the domain.

Appendix H.2. The likelihood function of the Bayesian inference problem

To setup the observation model, we measure the water table $u(s, X)$ at $m = 15 \times 15$ locations defined as the vertices of a uniform Cartesian grid on $D = [0, 1]^2$ with grid size $1/(\sqrt{m} + 1)$, as shown in Fig. 4. Each of the measurements is assumed to be corrupted by independent Gaussian observational noise. Using the partial differential equation (H.3), for a given realization of X , the observables are simulated numerically as the average of $u_h(s, X)$ over some subdomains $D_i \subset D$, $i = 1, \dots, m$, around the measurement locations. In our experiments, each D_i is a square with side length $2/(\sqrt{m} + 1)$ centred at the i th location. This leads to the parameter-to-observable map

$$y_i = Q_i(x) + \eta_i, \quad Q_i(x) = \frac{1}{|D_i|} \int_{D_i} u_h(s, x) ds, \quad \eta_i \sim \mathcal{N}(0, \sigma_n^2) \quad (\text{H.5})$$

for $i = 1, \dots, m$, where σ_n^2 is the variance of the measurement noise. For each parameter realization $X = x$, we need to first numerically solve (H.3) to obtain the water table $u_h(s, x)$, and then apply the same finite element discretization to calculate $Q(x)$ using the above formula. This gives the likelihood function,

$$\mathcal{L}^y(x) \propto \exp \left\{ -\frac{\|Q(x) - y\|_2^2}{2\sigma_n^2} \right\},$$

and the posterior distribution $\pi^y(x) \propto \mathcal{L}^y(x) \pi_0(x)$.

Appendix H.3. Additional experiments of the a posteriori risk estimation

Here, we provide additional numerical experiments for changing the risk threshold τ_* , the smoothing width γ^* , and the dimension of the truncated random field d . To enable the computations in a wide range of parameters, we change the smoothness parameter to $\nu = 2$, noise variance to $\sigma_n^2 = 10^{-2}$ and the correlation length to $\ell = 1$. With these parameters, the truncated representation of the dimension $d = 25$ can capture 99.99% of the variance of the infinite series (H.1). Moreover, we change the Dirichlet boundary conditions to $u|_{s_1=0} = 1$ and $u|_{s_1=1} = 0$. To apply Alg. 1, a fixed tensor rank 7 and bridging parameters $\beta_1 = 10^{-3}$, $\beta_{\ell+1} = \sqrt{10} \beta_\ell$, $\gamma_\ell = \beta_\ell \gamma^*$ and $\alpha_\ell = \beta_\ell$ are used throughout this set of experiments. We use a sample size of $N = 2^{15}$ in all experiments.

We first vary τ_* and calculate the *a posteriori* risks of breakthrough using a default smoothing width $\gamma^* = 100/\tau_*$. The results are shown in Fig. 8 together with Hellinger errors of the importance density functions used in the ratio estimator, as well as the total number of density evaluations needed in Alg. 1. As above, we consider three Hellinger errors: the distance $D_H(\bar{p}, p^*)$ between the computed deep importance density and the optimal importance density for the numerator of the ratio estimator, the distance $D_H\{\bar{p}, \phi_n^{(L)}\}$ between the deep importance density and the final layer of smoothed importance densities for the numerator of the ratio estimator, as well as the distance $D_H(\bar{q}, \pi^y)$ between the computed deep importance density and the optimal importance density for the denominator of the ratio estimator. Clearly

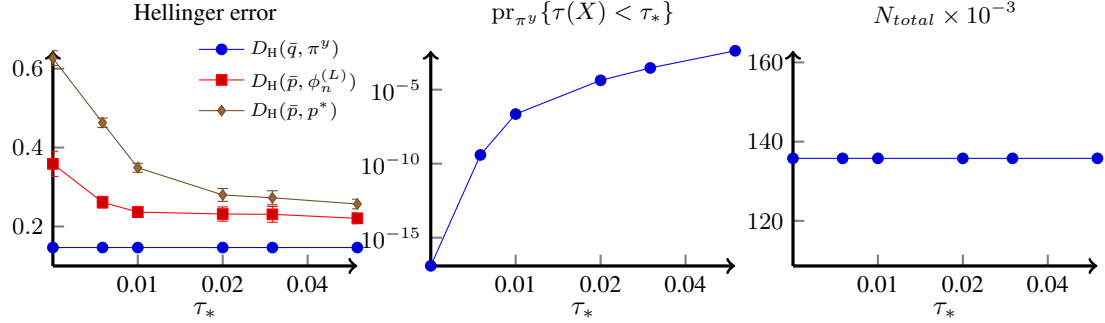


Fig. 8: Hellinger errors in the density approximations (left), *a posteriori* breakthrough probabilities (middle) and total number of density evaluations in Alg. 1 (right) for different breakthrough thresholds τ_* . Points denote average, and error bars denote one standard deviation over 10 runs.

smaller τ_* lead to smaller probabilities of a particle travelling through the channel in a time below τ_* . Consequently, the optimal importance density of the numerator becomes harder to approximate when τ_* decreases. Correspondingly, we observe that the Hellinger errors $D_H(\bar{p}, p^*)$ and $D_H\{\bar{p}, \phi_n^{(L)}\}$ increase as τ_* decreases. Nevertheless, even extremely small probabilities (below 10^{-10}) can be estimated accurately. For this set of experiments, the number of function evaluations stays constant, as the same parameters are used in Alg. 1.

Then, with a fixed risk threshold $\tau_* = 0.03$, we study the behaviour of Alg. 1 when the smoothing width γ^* and the tensor ranks are changed. The left plot of Fig. 9 shows the resulting Hellinger errors for approximating the optimal importance density of the numerator as a function of γ^* . The tensor-train approximation error increases with increasing γ^* due to the loss of smoothness, while the bias error between the exact optimal importance density p^* and the smoothed density $\phi_n^{(L)}$ decreases. Thus, there is an optimal γ^* to obtain the most accurate approximation of the optimal importance function $p^*(x)$, where the two error contributions balance. Regarding the dependency on the maximum rank r , for a fixed $\gamma^* = 100/\tau_*$ we observe that all Hellinger errors decay with r until the discretisation error is reached, whereas the number of function evaluations in Alg. 1 appears to depend quadratically on r , as expected from the number of degrees of freedom in the tensor-train decomposition.

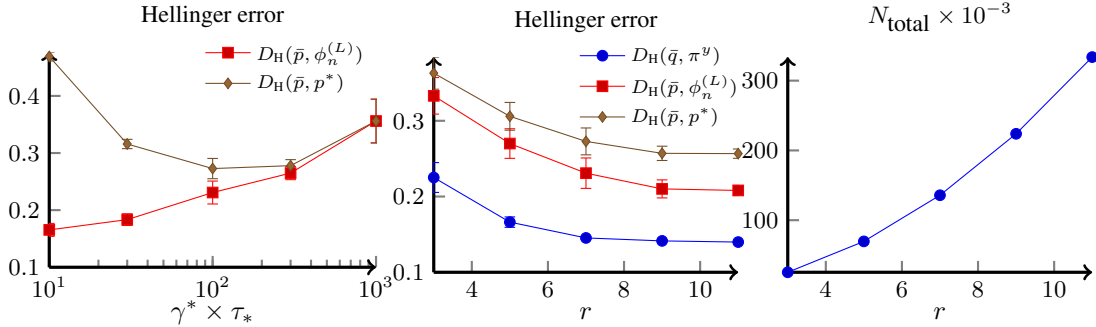


Fig. 9: Hellinger errors for *a posteriori* risk estimation for different smoothing widths γ^* (left) and tensor ranks r (middle) where $\tau_* = 0.03$. The right figure shows the total number of density evaluations in Alg. 1 as a function of the rank r for $\gamma^* = 100/\tau_*$. Points denote averages, and error bars denote one standard deviation over 10 runs.

Finally, we vary the dimension of the input random field from $d = 5$ to 25 and take the threshold $\tau_* = 0.15$ to test the dimension scalability of deep importance sampling for estimating the *a posteriori* risk. The

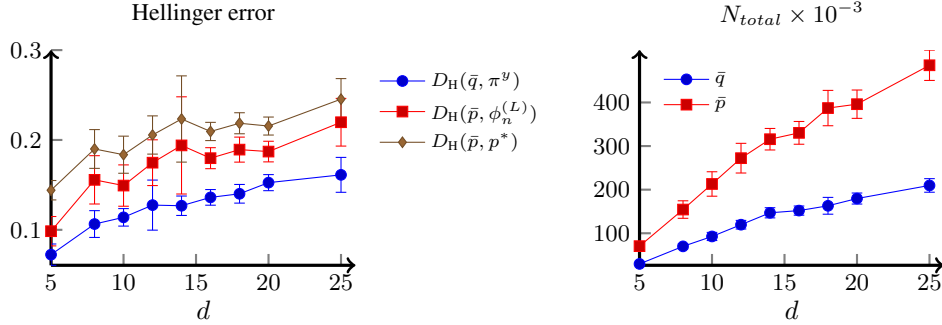


Fig. 10: Hellinger errors in the densities (left) and total number of function evaluations in Alg. 1 (right) for estimating the *a posteriori* risk in Example 2 with $\tau_* = 0.15$ and varying the parameter dimension d . Points denote averages, and error bars denote one standard deviation over 10 runs.

synthetic, observed data are generated using the diffusivity field with high diffusivity channel, depicted in the bottom of Fig. 4. The tensor ranks are adaptively chosen using 5 iterations of the cross algorithm, starting from rank 1 and increasing the ranks by at most 2 in each iteration to obtain a relative Frobenius-norm error below $3 \cdot 10^{-2}$. We use piecewise linear basis functions on 17 grid points to discretize the density in each coordinate direction, truncating the unbounded domain to $[-5, 5]$. We choose a smoothing width of $\gamma^* = 100/\tau_*$. The results are shown in Fig. 10. We observe that the computational complexity, measured in terms of density evaluations, depends no worse than linearly on the dimension, while the Hellinger error increases only logarithmically with respect to the dimension.

Appendix H.4. *A priori failure probability estimation*

We also compute the *a priori* risk and compare deep importance sampling with the cross entropy method. To apply Alg. 1, we compute the approximation of the optimal importance density with tensor rank $r = 9$, bridging parameters $\beta_1 = 10^{-2}$, $\beta_{\ell+1} = \sqrt{10} \beta_\ell$, $\gamma_\ell = \beta_\ell \gamma^*$, and two options for the smoothing width $\gamma^* = 30/\tau_*$ and $\gamma^* = 100/\tau_*$. This requires a total of $N_{total} = 159885$ density evaluations to construct the composite map. In the left plot of Fig. 11, we plot the Hellinger errors of the deep importance densities versus the risk thresholds τ_* . We consider two Hellinger distances: the distance $D_H(\bar{p}, p^*)$ between the computed deep importance density \bar{p} and the optimal importance density p^* , as well as the distance $D_H\{\bar{p}, \phi^{(L)}\}$ between the deep importance density \bar{p} and the final layer of smoothed importance densities $\phi^{(L)}$. As for *a posteriori* risk estimation above, smaller τ_* values lead to smaller probabilities of a particle travelling through the channel in a time below τ_* , which increases the difficulty to approximate the importance densities and is reflected in a higher Hellinger error.

In Fig. 12, we compare deep importance sampling to the cross entropy method of Botev & Kroese (2008), for the risk threshold fixed at $\tau_* = 0.03$. Here, the cross entropy method uses only one single Gaussian density, which is the best we were able to fit, while the smoothing width $\gamma^* = 100/\tau_*$ is used to build bridging densities for deep importance sampling in Alg. 1. We run 10 replicas of each method to estimate relative standard deviations of the risk probabilities, which are shown in the left plot of Fig. 12. In the right plot of Fig. 12, we also show the total number of density evaluations used by each of the methods. In this example, the cross entropy method is able to compute qualitatively correct risk estimates in higher dimensions, albeit requiring a larger number of density evaluations (starting from 2×10^5 samples per iteration at $d = 5$, growing to 6×10^5 for $d = 18$). However, for $d \geq 20$, the cross entropy method is unable to converge, even using $N = 10^6$ samples per iteration. In comparison, the number of density evaluations in deep importance sampling demonstrates a linear scaling in the dimension and nearly constant errors that are about two orders of magnitude below those of the cross entropy method. Moreover, this is achieved using one order of magnitude fewer density evaluations compared to the cross entropy method.

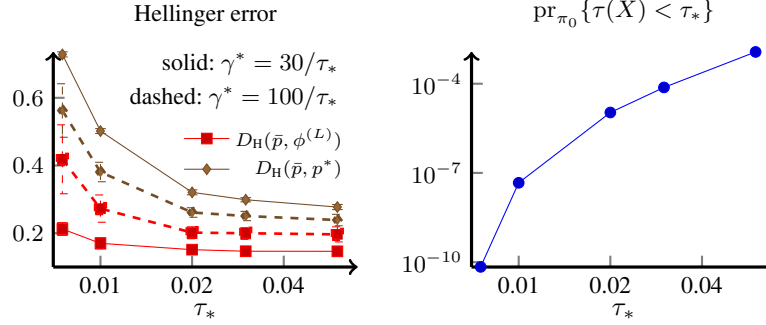


Fig. 11: Hellinger errors in computed deep importance densities for *a priori* risk estimation for different breakthrough time thresholds τ_* and smoothing widths γ_* (left), as well as the associated values of the *a priori* risk (right). Points denote average, and error bars denote one standard deviation over 10 runs.

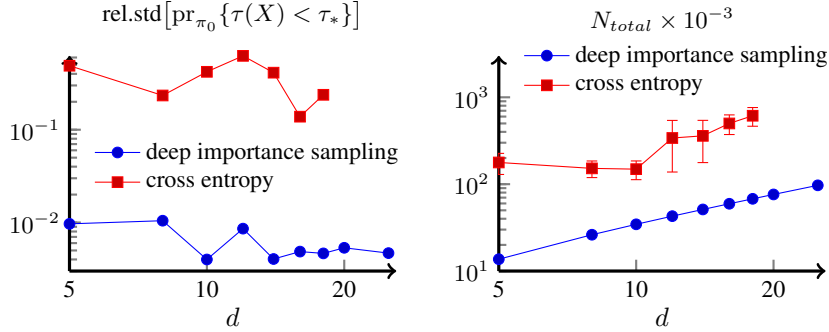


Fig. 12: Relative standard deviation of the *a priori* risk, estimated using 10 runs, comparing deep importance sampling and the cross entropy method (left), as well as total number of density evaluations used in each case (right).

[Received on T B A. Editorial decision on T B A]